J. Micropalaeontology, 44, 573–599, 2025
https://doi.org/10.5194/jm-44-573-2025

Journal of Micropalaeontology
Open Access

Chronostratigraphic ranges of Early–Middle Miocene larger benthic foraminifera calibrated by planktonic foraminiferal assemblages (Sierra de Marmolance, Granada, SE Spain)

Mónica Bolivar-Feriche[1], Jesús Reolid[2], Julio Aguirre[2], Davide Bassi[1], and Juan C. Braga[2]

[1]Dipartimento di Fisica e Scienze della Terra, Università degli Studi di Ferrara, Via Saragat 1, 44122 Ferrara, Italy
[2]Departamento de Estratigrafía y Paleontología, Universidad de Granada, Campus Fuentenueva, 18071, Granada, Spain

Correspondence: Davide Bassi (bsd@unife.it)

Received: 25 March 2025 – Revised: 7 October 2025 – Accepted: 19 October 2025 – Published: 25 November 2025

Abstract. An ∼300 m thick succession of bioclastic limestones and marls crops out in the Sierra de Marmolance (Subbetic Domain, External Zones, Betic Cordillera, SE Spain). Assemblages of planktonic foraminifera (PF) in the marls, underlying and laterally changing to limestones, indicate a late Burdigalian–early Serravallian age for the carbonates. Outcrop-scale geometry, stratigraphic patterns, facies distribution, and biogenic components reveal that Marmolance limestones formed on a prograding ramp with depth-related facies gradients. In the late Burdigalian–Langhian, from deeper to shallower, the facies are planktonic foraminiferal packstone and marls, *Nummulites* packstone, *Neorotalia* packstone, and lepidocyclinid packstone. In the early Serravallian, *Nummulites* packstone is missing and *Risananeiza* packstone and bioclastic rudstone with siliciclastics occur shorewards of lepidocyclinid packstone.

Altogether, 18 species of larger benthic foraminifera (LBF) were identified in the Marmolance succession. Among them, before the present study, *Nummulites fichteli*, *N. vascus*, *N. kecskemetii*, *Eulepidina dilatata*, *Eulepidina formosoides*, *Nephrolepidina praemarginata*, and *Risananeiza crassaparies* were considered exclusively Oligocene taxa, whereas *Nephrolepidina morgani*, *N. tournoueri*, *Neorotalia viennoti*, and *Spiroclypeus* sp. were supposed to disappear in the Early Miocene. In Marmolance, *Nummulites vascus* and *N.* cf. *kecskemetii* appear in Burdigalian and Langhian strata, whereas *N. fichteli* is only recorded in Langhian beds. *Eulepidina dilatata*, *E. formosoides*, *Nephrolepidina morgani*, *N. praemarginata*, *N. tournoueri*, *N. viennoti*, *Risananeiza crassaparies*, and *Spiroclypeus* sp. extend at least to the Serravallian. The presence of *Nummulites* in the Langhian of SE Spain partly fills the stratigraphic gap in the genus record from the end of the Oligocene to the living representatives in modern Indo-Pacific areas. These findings substantially modify the chronostratigraphic ranges and assumed diversity of Neogene LBF in the Mediterranean area.

1 Introduction

In the Western Tethys, Paleocene–Miocene shallow-water carbonates and mixed siliciclastic carbonates are characterized by highly diverse larger benthic foraminifera (LBF), some of which have been considered age-diagnostic markers. Drooger (1956) made the first attempt to correlate the Oligocene–Miocene LBF zones with the biostratigraphy of planktonic foraminifera (PF) in the Caribbean and European/Mediterranean domains. Blow (1957) questioned Drooger's (1956) correlation scheme based on new data of microfauna from Sicily and Malta and on new findings of *Miogypsina* spp. from NW Morocco. Following the biostratigraphic schemes of Hottinger (1960) based on alveoli-

noids, integrated nummulitid biozones embracing the Paleogene were proposed for the Mediterranean region (Hottinger et al., 1964). Such biozones were successively defined and implemented as shallow benthic zones (SBZs) for the Paleocene–Eocene (Serra-Kiel et al., 1998) and the Oligocene–Miocene (Cahuzac and Poignant, 1997). The Paleocene–Eocene SBZs, applied from the eastern Atlantic to the central Tethys (India), were in part tentatively correlated to magnetostratigraphic data from the Pyrenean domain (Serra-Kiel et al., 1998, 2020). The seven SBZs proposed by Cahuzac and Poignant (1997) represented the first attempt of an Oligocene–Miocene biozonation based exclusively on LBF, mostly from areas in western France (Cahuzac and Poignant, 1997, p. 157). These authors tentatively correlated their zones with the planktonic foraminiferal zonation of Blow (1969) and the calcareous nannoplankton zonation of Martini (1971).

The zones proposed by Cahuzac and Poignant (1997) were interval zones; therefore, their definition and identification were based on their bounding biohorizons, on first and last appearance data (i.e. FAD, LAD). The base of the Rupelian (SBZ 21) was identified by the FAD of *Nummulites fichteli* and *N. vascus*. Embracing the Rupelian–Chattian boundary, the base of SBZ 22 was defined by the FAD of *Eulepidina formosoides* and *Nephrolepidina praemarginata*, and the top was defined by the FAD of *Miogypsinoides*. The Oligocene–Miocene boundary (SBZ 23–24) was marked by the disappearance of *Nummulites*, *Cycloclypeus*, *Victoriella*, and *Praerhapydionina* and by the appearance of *Miogypsina* gr. *gunteri*. Records of *Cycloclypeus* from the Burdigalian of Aquitaine and Türkiye (Cahuzac and Poignant, 2004; Özcan and Less, 2009) and records of *Praerhapydionina* from the Burdigalian–early Langhian of Kurdistan (Al-Qayim et al., 2016) and from the Early Miocene of the Bahamas (BouDagher-Fadel, 2018) questioned the LAD of these genera at the Oligocene–Miocene boundary proposed by Cahuzac and Poignant (1997).

The Early–Middle Miocene boundary (SBZ 25–26) was defined by the extinctions of *Nephrolepidina* and miogypsinids in the Mediterranean region (Cahuzac and Poignant, 1997). In this region, the Langhian faunas were tentatively characterized by the occurrence of *Borelis* gr. *melo* (Cahuzac and Poignant, 1997, 1998). However, the taxonomic and biostratigraphic re-assessment of *Borelis melo* and *B. curdica* concluded that they reached the Tortonian and the Messinian, respectively (Betzler and Schmitz, 1997; Bassi et al., 2021a). This result agrees with Adams et al. (1983, p. 290), who stated that in the absence of control by PF, Langhian and Serravallian shallow-water successions could not be separated.

In general, the chronostratigraphic value of LBF FADs and LADs is not uniform, as they have intrinsic relationships to palaeoecology and palaeobiogeography (e.g. BouDagher-Fadel and Banner, 1999; Lunt and Allan, 2004; Renema, 2007; Bassi et al., 2024). Some LBF biozones have been based on FADs of morphospecies within evolutionary lineages according to morphometric limits (Less, 1987; Özcan et al., 2009a, b, 2010). However, defining biozones by the first occurrence of single species within a lineage may often be a matter of interpretation and a source of error (Lunt and Allan, 2004; BouDagher-Fadel and Price, 2021). Last-appearance data are even more questionable due to taphonomic, ecological, and biogeographical factors. In any case, as claimed decades ago by Adams et al. (1983) and Drooger and Laagland (1986), there is a need to test the proposed chronostratigraphic ranges of LBF taxa in the Oligocene–Miocene of the Mediterranean region with approaches allowing correlation with the standard chronostratigraphic scale based on PF zonal schemes.

Shallow-water limestones rich in LBF crop out in the Sierra de Marmolance, in the External Zones of the Betic Cordillera (SE Spain) in the western Mediterranean (Fig. 1). These carbonates were initially attributed to the Eocene by Fallot (1945), although some years later Foucault (1960, 1971) suggested an Early Miocene age for the bulk of them. The record of PF assemblages in marls underlying and laterally changing to the shallow-water limestones allows a re-assessment of the chronostratigraphic ranges of some Miocene LBF species. The results entail significant changes in the up-to-now assumed last occurrence ages of LBF species used as biozone markers in currently applied SBZ schemes. They also imply a substantial improvement in the understanding of palaeobiogeographical dynamics of LBF in the Mediterranean area after the Burdigalian closure of the Tethyan Seaway (Piller et al., 2024).

2 Geological setting

The Sierra de Marmolance (Marmolance hereinafter) belongs to the External Zones of the Betic Cordillera (southern Spain; Fig. 1), which is the westernmost segment of the European Alpine belt. The External Zones of the cordillera are a thin-skinned thrust belt composed of Mesozoic to Middle Miocene sediments accumulated on the southern margin of the Iberian plate (García-Hernández et al., 1980). Two other major tectonic domains are identified in the Betic Cordillera: the Internal Zones, formed by the superposition of tectonic complexes, mainly composed of Paleozoic to Mesozoic metasediments (Jabaloy et al., 2019), and the Flysch Units, comprising Upper Cretaceous to Middle Miocene allochthonous deposits accumulated in deep-sea fans (Jabaloy et al., 2019; Sanz de Galdeano and Vera, 1992).

The External Zones are divided into the Prebetic and Subbetic domains. The Prebetic Domain was the closest to the Iberian palaeomargin and is characterized by continental and shallow-marine sedimentation. In contrast, after a continental–shallow-marine phase from the Triassic to the Lower Jurassic, pelagic marine sedimentation prevailed in the distal Subbetic Domain (García-Hernández et al., 1980).

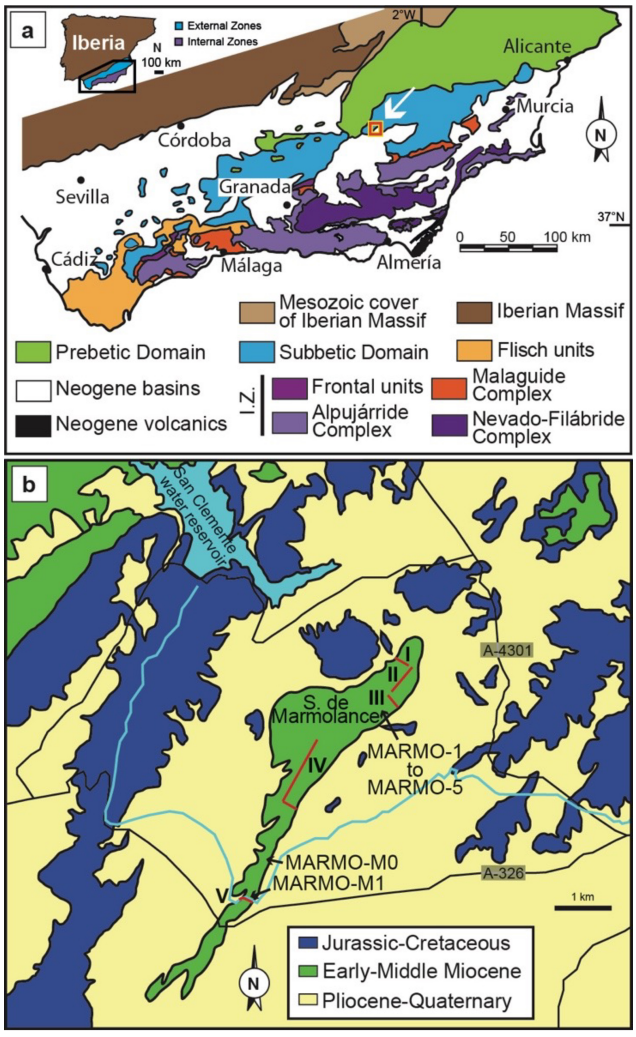

Figure 1. **(a)** Geological map of the Betic Cordillera. The red square indicates the location of the map in panel **(b)**. I.Z.: Internal Zones. Modified from Foucault (1974). **(b)** Geological map of the Sierra de Marmolance area with the location of logged stratigraphic sections (red lines I–V), the location of marl samples with planktonic foraminifera (MARMO-1 to MARMO-5, MARMO-M0, and MARMO-M1), and access roads (black lines). The blue line is a water channel. Simplified from Lupiani-Moreno et al. (1994a, b).

This long-lasting configuration changed in the Miocene due to the folding, thrusting, and uplift of Prebetic and Subbetic nappes caused by the westward–northwestward collision of the Internal Zones with the southern Iberian margin (Jabaloy et al., 2019).

During the Miocene, the uplift of some areas in the Subbetic Domain led to the development of shallow-water shelf deposits, such as the ones forming Marmolance (Fig. 1). Since the late Tortonian (Late Miocene), the N–S general compressional regime due to the convergence of African and Eurasian plates configured the major Subbetic reliefs as antiforms trending E–W to ENE–WSW (Sanz de Galdeano and Alfaro, 2004; Galindo-Zaldívar et al., 2019).

3 Materials and methods

The Sierra de Marmolance is a carbonate ridge that extends around 7.5 km with an orientation approximately N035E to N030E (Fig. 1). The best exposures occur at the southeastern slope of the ridge, along a nearly vertical wall around 5.9 km long (Fig. 2). An ∼ 300 m thick succession of Lower–Middle Miocene bioclastic limestones and marls builds the ridge. The succession was logged in five sections, whose locations were conditioned by accessibility and quality of exposure. They comprise three sections in the eastern part (sections I to III) and one composite (Section IV) and a short section (San Clemente channel, Section V) in the western part. The central part of the ridge was not sampled because of landslides and inaccessible cliffs. A correlation of sections was visually made by following bedding along the southeastern side of the ridge (Figs. 2–5). The long distances between sections and exposure gaps introduced some degree of uncertainty in the correlation, which, however, is not higher than ±10 m. Quaternary materials and debris cover the succession at the lower ridge slopes, making it difficult to follow the lateral continuity of strata at the base of the slope in the marly deposits and precluding the systematic sampling of the marls.

The studied materials (thin sections and isolated PF specimens) are stored in the collections of the Departamento de Estratigrafía y Paleontología, labelled as "Miocene_Marmolance", accessible to any interested scientist.

3.1 Planktonic foraminifera

Marls underlying and interfingering with limestones were sampled to analyse their PF content to constrain the age of the succession. Planktonic foraminiferal biostratigraphy is based on five stratigraphically close marl samples collected at the northeastern slope of the ridge (MARMO-1 to MARMO-5) and on two marl samples taken in the southwestern part of the Marmolance (MARMO-M0 and MARMO-M1). They correspond to marls outcropping in the lower part of carbonate succession and in the initial steps of progradation (MARMO-1 to MARMO-5) (Fig. 2c) and to marls intercalated in limestone beds in the middle part of the limestone stack (MARMO-M0 and MARMO-M1) (Fig. 2d). Marls below the carbonates are cemented, fractured, and covered by vegetation and scree debris (Fig. 2c, e), precluding a systematic and regularly spaced sampling. We obtained the samples from the less cemented and best exposed areas, allowing us to date the beginning of the carbonate deposition.

All samples were sieved with 0.25 and 0.125 mm meshes. The residue above 0.125 mm was dried in an oven at 40 °C and examined for biostratigraphic results. Taxonomic classification of the PF was based on Kennett and Srinivasan

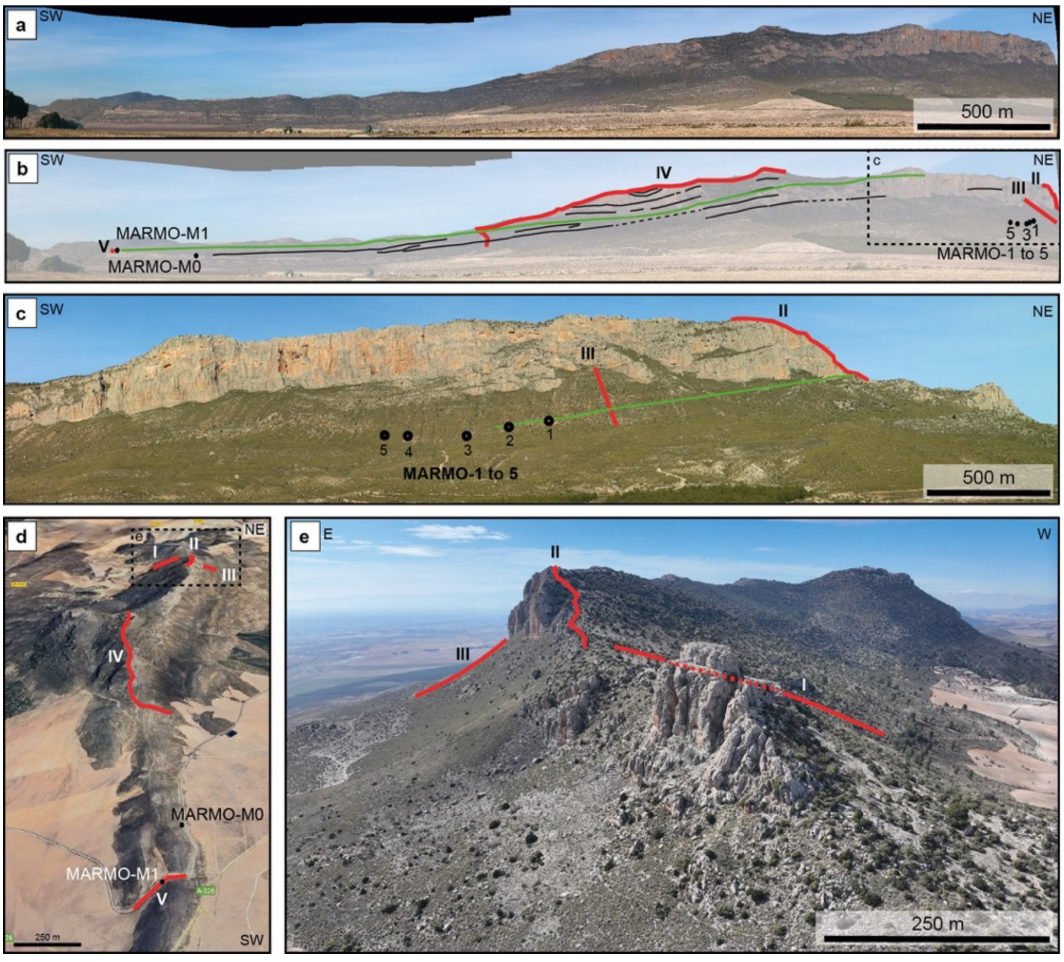

Figure 2. **(a)** Panoramic view of the southern slope of the Sierra de Marmolance. The limestone exposures on the slope are ~ 5.9 km long. **(b)** Locations of the logged sections (red lines I–V) and of marl samples with planktonic foraminifera (MARMO-1 to MARMO-5, MARMO-M0, and MARMO-M1). The green line marks the visual correlation of the Langhian–Serravallian transition (sample MARMO-M1) with beds along the panoramic. Black lines depict bedding surfaces traceable for hundreds of metres to kilometres. The dashed square indicates the location of panel **(c)**. **(c)** Panoramic view of the eastern end of the southern slope of the Sierra de Marmolance with the locations of sections II and III (red lines) and marl samples MARMO-1 to MARMO-5. The green line depicts the visual correlation of the Burdigalian–Langhian transition with beds in sections II and III. **(d)** Aerial view of the Sierra de Marmolance from the SW with the locations of logged sections (red lines I–V) (from © Google Earth 2025). **(e)** Aerial view of the NE end of the Sierra de Marmolance with the locations of sections I–III (red lines). The dashed interval in Section I indicates its trace hidden by the hill in the foreground.

(1983), Bolli and Saunders (1985), Iaccarino (1985), Young et al. (2017), and Wade et al. (2018). Selected specimens were observed and photographed in an environmental scanning electron microscope FEG-ESEM QemScan650F (Centro de Instrumentación Científica, Universidad de Granada).

The biostratigraphic scales proposed by Lirer et al. (2019) for the Mediterranean and by Wade et al. (2011) for the low-latitude open-ocean PF were followed. Wade et al. (2011) proposed an integrated revised biostratigraphy based on low-latitude (tropical–subtropical) open-ocean areas valid worldwide. In the Mediterranean, Lirer et al. (2019) proposed a different Neogene foraminiferal biozonation almost exclusively based on type sections located in Italy, central Mediterranean. The only exceptions are the DSDP 372 section (Balearic Basin), the Oued Akrech section (Rabat, NW Morocco), and the Abad section (Sorbas Basin, SE Spain, western Mediterranean). The last two sections were considered to characterize the Tortonian–Messinian boundary and Messinian biozones.

Due to Mediterranean provincialism, both Neogene biozonation schemes generally use different biomarkers, resulting in different biozonal frameworks (Wade et al., 2011; Lirer et al., 2019). In addition, when considering the same species to characterize biozonal boundaries, the age of the biomarkers differs in both scales (Fig. 6).

The Marmolance carbonates were deposited in the western Mediterranean in a basin connected with the Atlantic and partially coinciding with the Miocene climatic optimum (MCO),

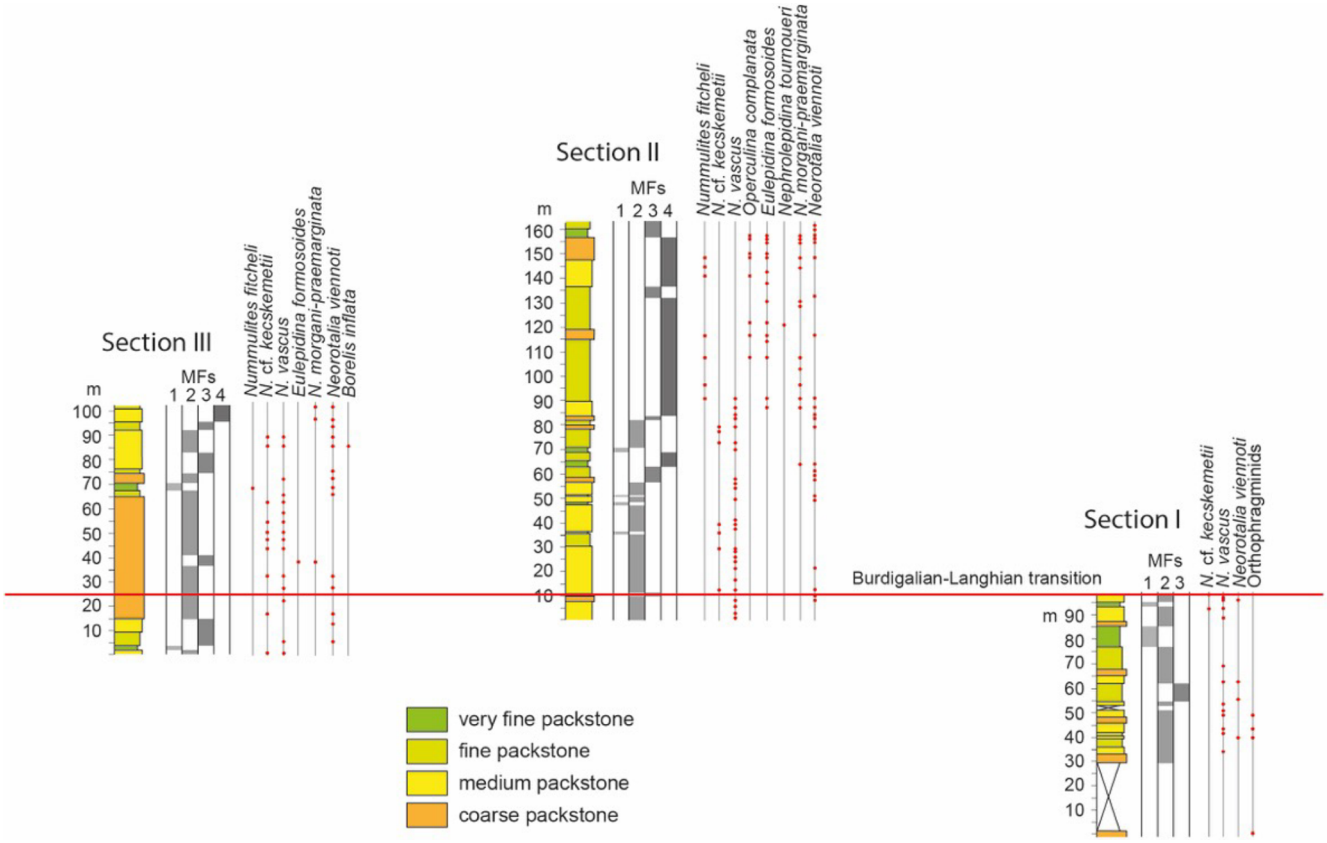

Figure 3. Lithofacies and LBF distribution in the eastern Marmolance sections. The correlation between columns was visually determined. The locations of the Burdigalian–Langhian and Langhian–Serravallian transitions were based on planktonic foraminiferal assemblages. MFs are facies distinguished based on fossil components.

when coral reefs and other tropical marine invertebrates developed in the Central Paratethys (Perrin and Bosellini, 2012; Harzhauser et al., 2025; Reuter et al., 2025). Therefore, Marmolance was under the influence of tropical–subtropical PF. The frequent occurrence of low-latitude forms of the *Fohsella* lineage (e.g. *F. peripheroronda* and scarce *F. peripheroacuta*) in the study samples account for this influence. In fact, the last occurrence of *F. peripheroronda* (as *Globorotalia peripheroronda*) is considered to define the top of the biozone MMi5 (early Serravallian; 13.5 Ma) in the Lirer et al. (2019) biozonation (Fig. 6). The same applies to the low-latitude species *Globorotalia praemenardii* (Kennett and Srinivasan, 1983; Aze et al., 2011), whose first occurrence is used to delimit the base of the biozone MMi5c (uppermost late Langhian; 13.92 Ma) in the Lirer et al. (2019) biostratigraphy (Fig. 6).

Another difference between the Lirer et al. (2019) and Wade et al. (2011) biozonations is that, in the Mediterranean, Neogene bioevents are both first/last common/regular occurrences of species and maximum abundances (acme zones) of individual species (Lirer et al., 2019). The correct application of these bioevents requires systematic and spaced sampling along PF-bearing sequences and that quantitative analyses of the relative abundance of species are made. Due to the difficulties of doing such a regular sampling in our study case, the application of those bioevents was unfeasible. In contrast, Wade et al. (2011) recognize first and last occurrences of specific biomarkers, which are more straightforwardly applicable in Marmolance. Taking into account the aforementioned issues, we use the Wade et al. (2011) biozone scheme and discuss the results with the bioevents recorded in the Lirer et al. (2019) standard biostratigraphic scale.

3.2 Larger benthic foraminifera and coralline red algae

All LBF-bearing deposits are hard-cemented limestones from which 229 rock samples were collected and prepared in 339 thin sections (47 × 27 mm in size). No isolated LBF specimens were found.

The taxonomy of *Nummulites* species follows Schaub (1981), Less et al. (2008), and Özcan et al. (2009a, b). Oligocene *Nummulites* species have been re-assessed according to dimensions of some test characters measurable at equatorial sections of A-forms (Drooger et al., 1971; Less, 1999; Less et al., 2006; Özcan et al., 2010). The species circumscriptions partly correspond to those proposed by

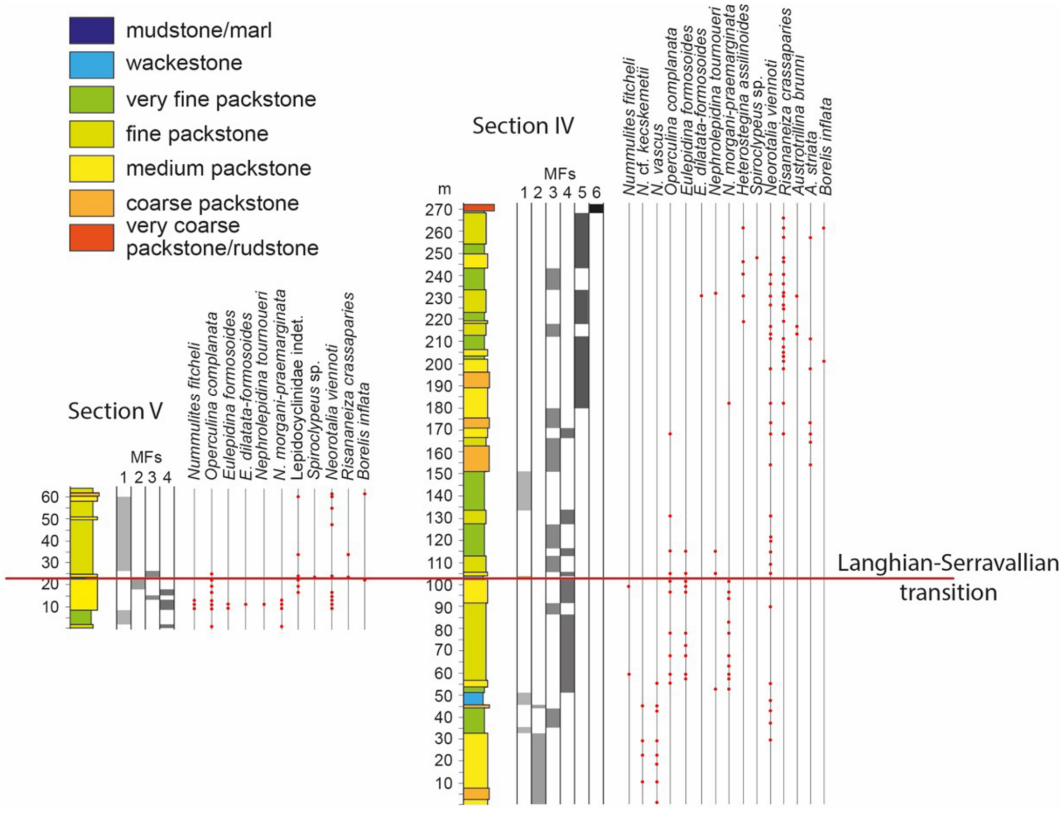

Figure 4. Lithofacies and LBF distribution in the western Marmolance sections. The correlation between columns was visually determined. The location of the Langhian–Serravallian transition was based on planktonic foraminiferal assemblages. MFs are facies distinguished based on fossil components.

Schaub (1981) (see also Serra-Kiel et al., 2016). The absence of isolated *Nummulites* specimens hampered the preparation of oriented sections (i.e. equatorial, axial). Three shell parameters from nearly equatorial sections were used to separate species: shell diameter (D), inner cross-diameter of the proloculus (P), and average length of chambers in the third whorl (Less et al., 2008; Özcan et al. 2009a, b).

Taxonomic circumscriptions for *Eulepidina* species follow van Heck and Drooger (1984), Less (1991), Özcan et al. (2009a, 2010), and Less et al. (2018), whereas for *Nephrolepidina* species de Mulder (1975) was followed. The terminology and parameters used to distinguish the species are those proposed by van der Vlerk (1959), Drooger and Socin (1959), and Özcan et al. (2009a). The Marmolance specimens of *Eulepidina* correspond to the main *formosoides–dilatata* Mediterranean lineage. The parameters used here to distinguish the species *E. formosoides* and *E. dilatata* are D (the average size of the deuteroconch) and A (the average degree of embracement of the protoconch by the deuteroconch), following the morphometric limits proposed by Özcan et al. (2009a, 2010) as to $D_{mean} = 1250\,\mu m$ and $A_{mean} = 83$. Linages are used for biostratigraphic purposes, following the artificial separation of species by arbitrary biometric limits based on numerical parameters, which are characteristic of each chronospecies (Özcan et al., 2009a, 2010). Sometimes the mean parameter of an assemblage can be very close to the limit between two neighbouring species. In this case, we adopt the proposal of Drooger (1993) by using an intermediate notation (the notation *exemplum intercentrale*, abbreviated as *ex. interc.*), followed by the names of the two species on either side of the limit, naming first the assemblage that is closer. For example, specimens from Marmolance were ascribed to *Eulepidina* ex. interc. *dilatata* et *formosoides*, since they show intermediate characteristics between *E. dilatata* and *E. formosoides*, being closer to the former. Taxonomic criteria adopted for porcelaneous LBF species are after the taxonomic re-assessments by Bassi et al. (2021a, b).

Taphonomic grades were assessed on LBF random sections. Water turbulence causes abrasion and fragmentation on LBF tests (e.g. Yordanova and Hohenegger, 2002; Beavington-Penney, 2004; Bassi et al., 2013). Subglobular and inflated lenticular LBF tests are more prone to be abraded, whereas flat tests are more fragile and easily underwent fragmentation (Hohenegger and Yordanova, 2001; Yordanova and Hohenegger, 2002). The degree of abrasion and fragmentation ranges from very well preserved (no abra-

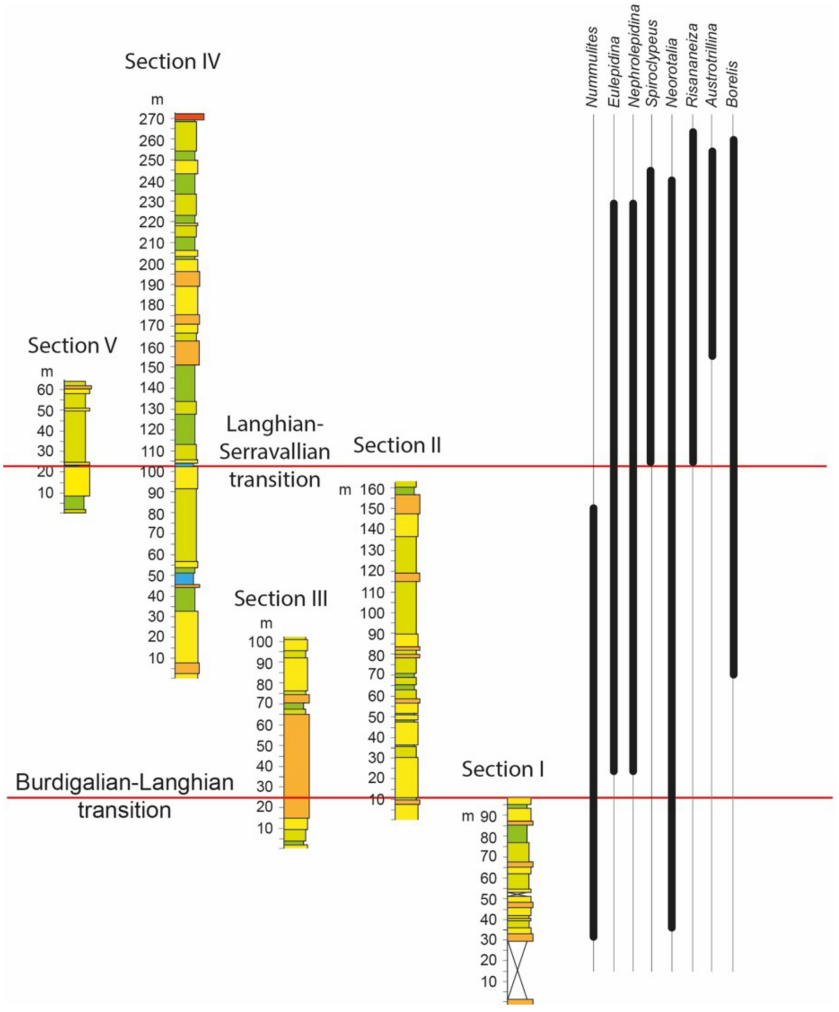

Figure 5. Visual correlation of logged sections with ranges of recorded LBF genera. The locations of the Burdigalian–Langhian and Langhian–Serravallian transitions were based on planktonic foraminiferal assemblages.

sion and fragmentation), through slightly abraded, moderately abraded, to highly abraded and fragmented.

Identifications of coralline red algae were based on preserved morpho-anatomical diagnostic characters. Taxonomy of family to order levels follows recent molecular phylogenies (Peña et al., 2020; Jeong et al., 2021). Bassi et al. (2000) and Vannucci et al. (2000) were followed to identify the fossil species *Subterraniphyllum thomasii*.

3.3 Facies analysis

Facies were quantitatively analysed in 147 thin sections representative of those qualitatively distinguished in the field and hand samples. Component proportions were estimated by point-counting in high-quality thin-section scans (2400 dpi resolution). In each thin section, 300 points were identified and counted with the random point-counting tool of JMicroVision software.

Statistical analyses were performed with the PAST software. The identified facies types were separated by cluster analysis based on LBF components and on PF and siliciclastic proportions. The cluster analysis performed followed the paired-group algorithm (UPGMA) and the Bray–Curtis similarity index. Other biogenic components, such as coralline algae and corals, even if abundant, were not considered in the cluster analysis, as their proportions did not significantly change among facies types. The statistical significance of the identified facies types was tested by one-way ANOVA (Table S1). The LBF considered for the statistical analyses were *Acervulina*, *Amphistegina*, *Austrotrillina*, *Borelis*, *Heterostegina*, lepidocyclinids, *Neorotalia*, *Nummulites*, *Operculina*, *Peneroplis*, *Risananeiza*, and *Spiroclypeus*. The LBF with abundance $< 1\,\%$ (*Haddonia*, *Sphaerogypsina*) were removed from the analysis. Component proportions are illustrated as Pareto charts ordered from highest to lowest. Components representing 80 % of the total are considered the

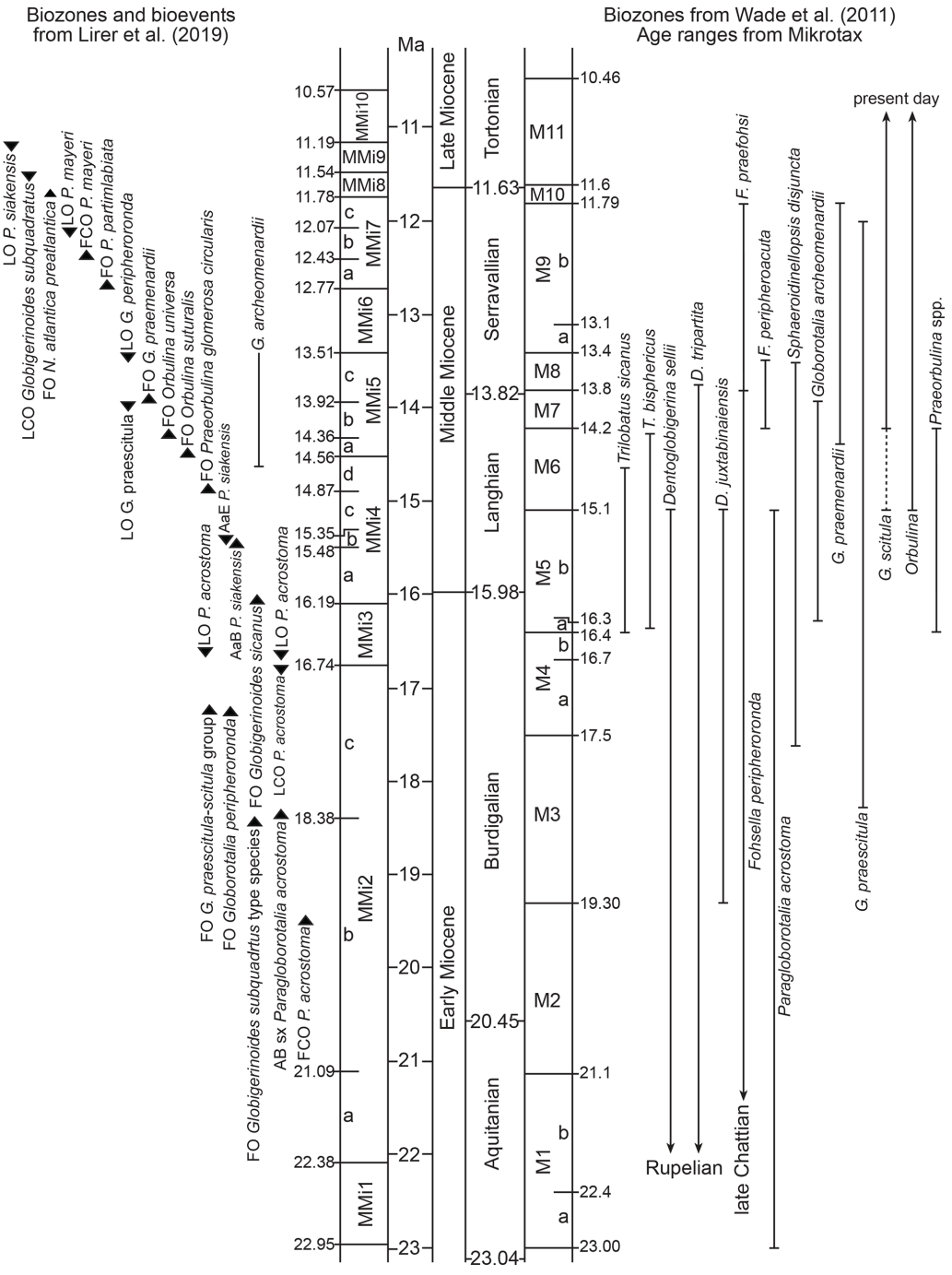

Figure 6. Biozone schemes of Lirer et al. (2019) and Wade et al. (2011). Age ranges of planktonic foraminifera species in Wade et al. (2011) biozones from MIKROTAX (Young et al., 2017). Symbols of the Lirer et al. (2019) scale: FO, first occurrence; FCO, first common occurrence; LO, last occurrence; LCO, last common occurrence; AB sx, acme bottom dominated by left-coiled forms; AaB, acme bottom; AaE, acme end. Timescale after Cohen et al. (2025).

dominant ones, whereas the remaining 20 % is subordinate (Table S1, Supplement).

4 Results

4.1 Lithology and general stratigraphic patterns

The Sierra de Marmolance is a ridge built by a thick (∼ 300 m) succession of limestone beds gently dipping to the W–SW and laterally changing to marls towards the SW (Fig. 2). On the southeastern slope of the ridge, this lateral change depicts a progradation toward the SW of limestones over marls. The carbonates are mostly bioclastic (wackestone to rudstone) with an increase in the terrigenous content toward the top of the succession (Figs. 3–4). Six facies were distinguished on the basis of field observations and quantification of component proportions of selected samples, under the microscope (Fig. 6; Table S1).

4.2 Planktonic foraminiferal biostratigraphy

All studied samples, except MARMO-M0, are rich in PF. Nonetheless, they are preserved as recrystallized inner casts and often deformed, hindering their identification. Samples MARMO-1 to MARMO-5 show similar PF content, including *Globigerinoides* spp., *Trilobatus trilobus*, *T. sicanus/T. bisphericus*, *Globoquadrina dehiscens*, *Globigerinita glutinata*, *Paragloborotalia continuosa*, *P. siakensis/P. mayeri*, *P.* cf. *acrostoma*, *Praeorbulina glomerosa*, *Globorotalia archeomenardii*, *G. praescitula*, *Dentoglobigerina venezuelana*, *D. baroemoenensis*, *D. juxtabinaiensis/D. selli*, *D. tripartita*, and *Sphaeroidinellopsis* cf. *disjuncta* (Fig. 7). Closely related and morphologically similar species cannot often be confidently separated due to preservation. In these cases, we use slash to indicate uncertainty among two species. Together with the aforementioned species, there are some specimens doubtfully attributed to ?*Globigerinatella* sp. We use a question mark because intense recrystallization of the moulds precludes a clear observation of the secondary areal apertures, making their identification very problematic.

The co-occurrence of *Trilobatus sicanus/T. bisphericus*, *Globorotalia archeomenardii*, *Praeorbulina glomerosa*, and *Dentoglobigerina juxtabinaiensis/D. selli* in samples MARMO-1 to MARMO-5 indicates the Burdigalian–Langhian transition, biozone M5b of Wade et al. (2011) (Fig. 6). This biozone correlates with the topmost biozone MMi3-middle part of the subzone MMi4c interval of Lirer et al. (2019). The first occurrence of *Trilobatus sicanus* (as *Globigerinoides sicanus*) in the Mediterranean marks the top of the biozone MMi3 (Lirer et al., 2019), slightly postdating the appearance of the nominal species in low-latitude open-ocean regions, but within the biozone M5 (Fig. 6).

According to Lirer et al. (2019), the total range of *Globorotalia archeomenardii* is between the top of biozone MMi4 and the top of biozone MMi5 (late Langhian–early Serravallian; Fig. 6). That is, in the Mediterranean, this species postdates the last occurrence of *D. juxtabinaiensis/D. selli* and the last occurrence of *Trilobatus sicanus/T. bisphericus* according to Young et al. (2017; Fig. 6). Influxes of *G. archeomenardii* from Atlantic low-latitude regions in Marmolance might account for this chronological discrepancy. The first occurrence of *P. glomerosa* in the open ocean delimits the lower boundary of the subzone M5b of Wade et al. (2011). Nonetheless, in the Mediterranean, the species slightly postdates the top of biozone M5.

The last occurrence of *Paragloborotalia* cf. *acrostoma* (Fig. 7h) took place within the base of the biozone MMi3, at the latemost Burdigalian in the Mediterranean (Lirer et al., 2019; Fig. 6). Nonetheless, in tropical–subtropical regions it disappeared at the top of M5 biozone (Young et al., 2017). The presence of this species in Marmolance, although its identification can be uncertain due to preservation, suggests Atlantic influxes. Planktonic foraminifera in sample MARMO-M0 were scarce and taphonomically greatly modified. We only identified *T. sicanus/T. bisphericus* and *Fohsella* cf. *peripheroronda*. Therefore, the sample cannot be confidently dated. Finally, MARMO-M1 contains abundant and well-preserved PF. This sample is dominated by paragloborotaliids (*Paragloborotalia continuosa*, *P. siakensis/P. mayeri*) and dentoglobigerinids (*Dentoglobigerina venezuelana*, *D. baroemoenensis*, *D. tripartita*). It also contains *Globigerinoides* spp., *Trilobatus trilobus*, *Globorotalia praemenardii*, *G. praescitula/G. scitula*, *Fohsella peripheroronda*, and rare specimens of *F. peripheroacuta* (Fig. 8).

The presence of *F. peripheroronda* and *F. peripheroacuta* in MARMO-M1 indicates that this sample can be attributed to the biozone M7, Langhian–Serravallian transition, of Wade et al. (2011; Fig. 6). In the Mediterranean, *F. peripheroacuta* is very rare and not considered in the biozonation, but the last occurrence of *F. peripheroronda* marks the top of biozone MMi5 (Lirer et al., 2019), embracing the late Langhian–early Serravallian transition within the age range of the biozone M7 (Fig. 6). Lirer et al. (2019) recognized a second acme of *P. siakensis* in the biozone MMi6 (early Serravallian) as an auxiliary biohorizon. This species is abundant in MARMO-M1, consistent with the assigned age.

4.3 Facies

4.3.1 Biotic components

Biotic components are dominated by coralline red algae, LBF (Figs. 10–12), and corals, with different proportions along the studied sedimentary successions (Table S1). Bivalves, bryozoans, and echinoderms are subordinate. Although often well preserved, components are heterometric and unsorted, and they show taphonomic alteration due to fragmentation and abrasion.

Coralline algae are the most abundant components in all facies except in distal planktonic foraminiferal packstones.

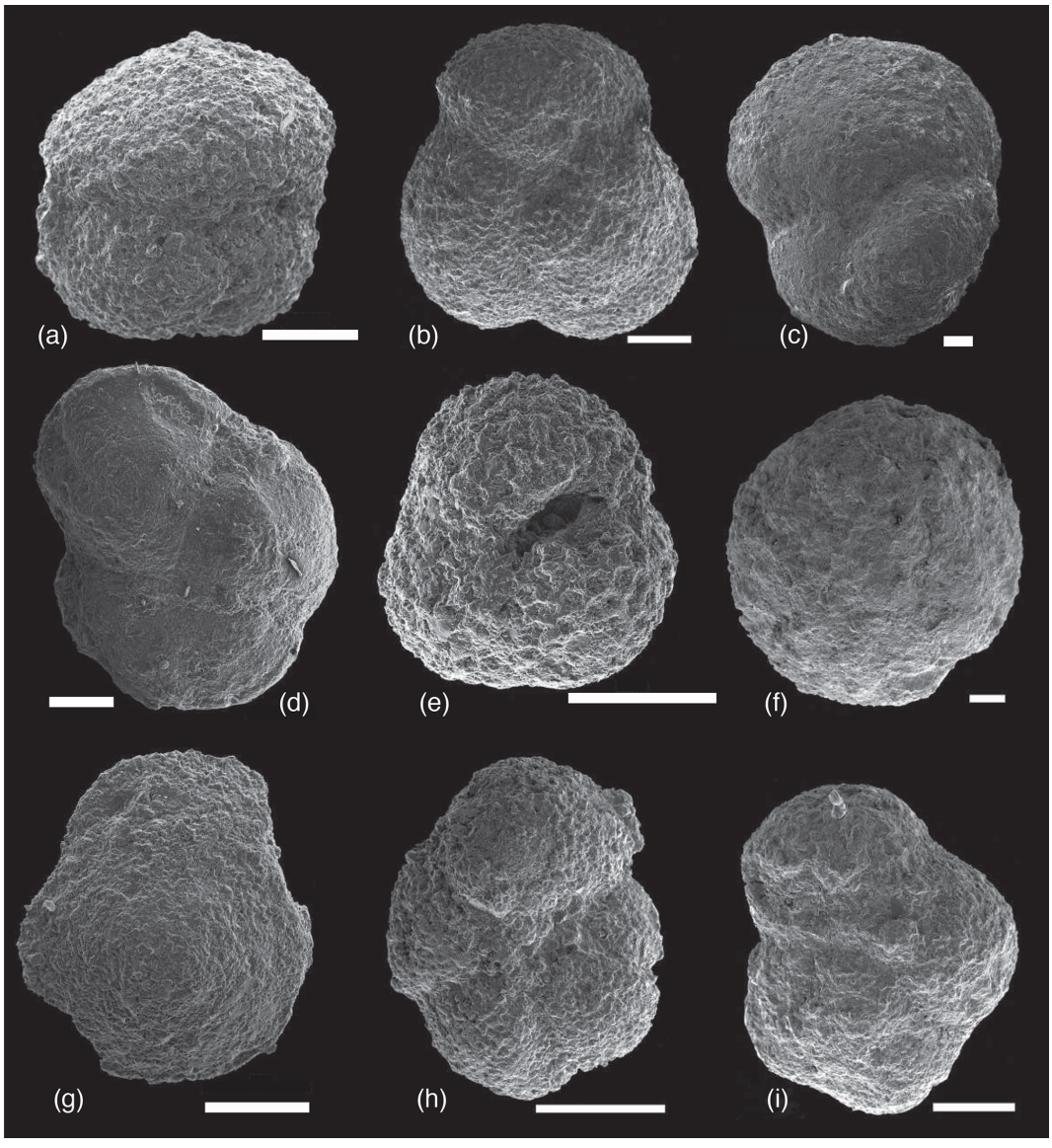

Figure 7. **(a)** *Dentoglobigerina juxtabinaiensis/D. selli*, umbilical view (MARMO-3). **(b)** *Dentoglobigerina tripartita*, umbilical view (MARMO-4). **(c)** *Trilobatus sicanus/T. bisphericus*, umbilical view (MARMO-4). **(d)** *Globorotalia archeomenardii*, umbilical view (MARMO-4). **(e)** *Sphaeroidinellopsis disjuncta*, umbilical view (MARMO-3). **(f)** *Praeorbulina glomerosa* (MARMO-3). **(g)** *Globorotalia praescitula/G. scitula*, dorsal view (MARMO-M1). **(h)** *Paragloborotalia* cf. *acrostoma*, umbilical view (MARMO-1). **(i)** *Paragloborotalia continuosa*, dorsal view (MARMO-3). The scale bar represents 100 µm in panels **(a)**–**(c)** and panels **(e)**–**(i)** and 150 µm in panel **(d)**.

They occur mostly as fragments and, less frequently, as rhodoliths. Most of them belong to the order Hapalidiales, with *Mesophyllum* being the most abundant genus, followed by *Lithothamnion*. Subordinate *Sporolithon*, *Lithoporella*, *Subterraniphyllum thomasii*, and several other geniculate species complete the coralline algal assemblages. The encrusting foraminifer *Acervulina* contributes to rhodolith formation.

Bivalves are present throughout the section, becoming larger and more abundant towards the top, where oyster fragments occur. Bryozoans occur as isolated fragments or encrusting coral branches and coralline algal thalli. Fragments of echinoderms are more common in the middle–upper part of the succession. Barnacles mostly appear together with oysters. Other components include small benthic foraminifera (rotaliids, miliolids, textulariids), planorbulinids, victoriellids, agglutinated encrusting foraminifera (*Haddonia* sp.), brachiopods, the serpulid *Ditrupa*, and the green alga *Halimeda*.

Terrigenous grains, mainly quartz, occur in the middle and upper parts of the succession, being more abundant and larger towards the top.

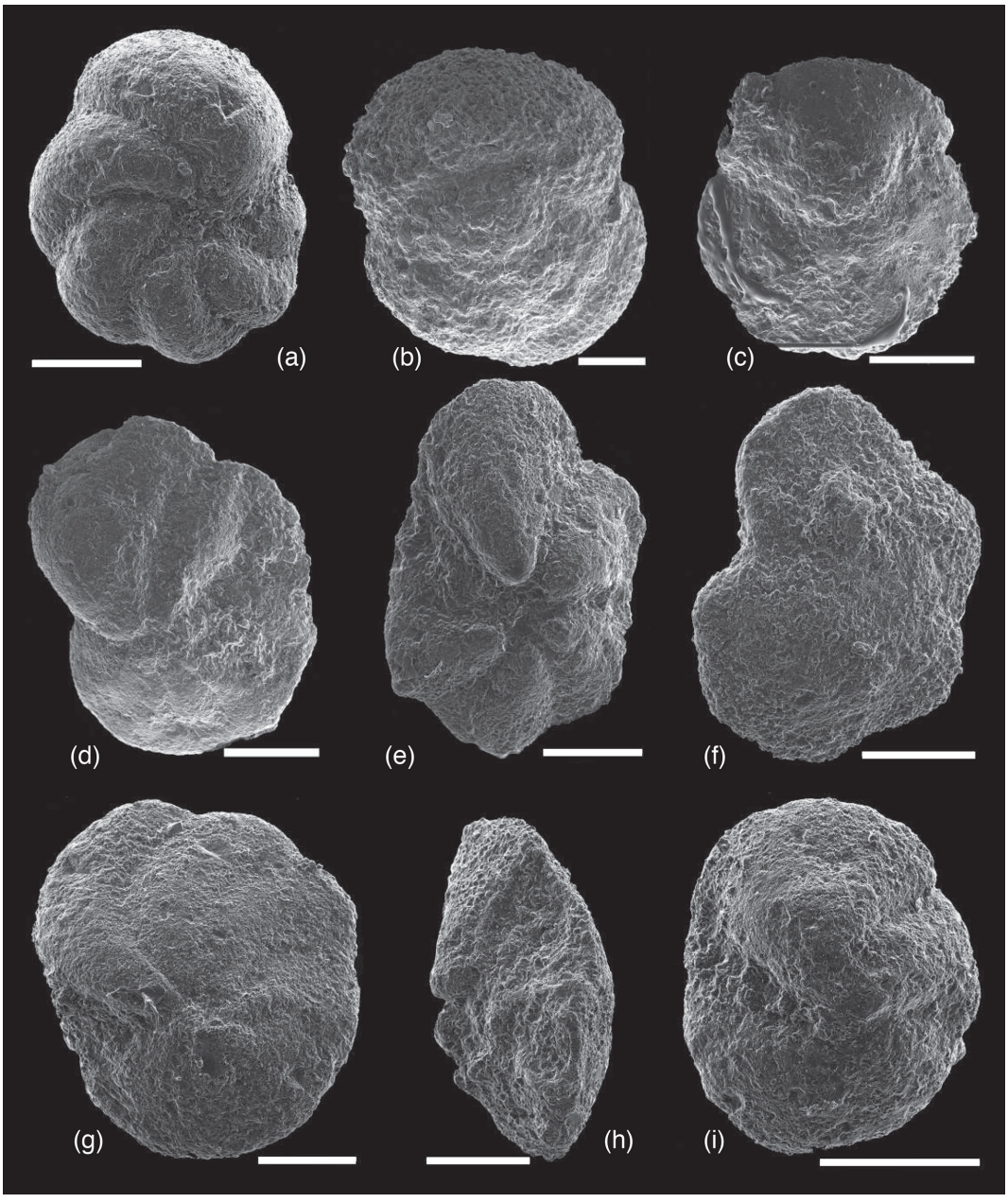

Figure 8. Planktonic foraminifera from sample MARMO-M1. **(a)** *Fohsella peripheroronda*, umbilical view. **(b)** *Dentoglobigerina tripartita*, dorsal view. **(c)** *Globorotalia praescitula/G. scitula*, umbilical view. **(d–i)** *Fohsella peripheroacuta*, dorsal view **(f)**, lateral view **(h)**, and umbilical view **(d, e, g, i)**. Scale bar represents 100 µm.

Six facies were distinguished: planktonic foraminiferal wackestone–packstone, *Nummulites* packstone, *Neorotalia* packstone, lepidocyclinid packstone, *Risananeiza* packstone, and bioclastic packstone with quartz. The distribution of facies in the studied stratigraphic sections is shown in Figs. 3–5. The distribution of components within the distinguished facies is shown in Fig. 9 and Table S1.

4.3.2 MF1, planktonic foraminiferal wackestone–packstone

The main components are PF and fragments of coralline algae with subordinate fragments of echinoderms and bryozoans. *Nummulites fichteli*, small benthic foraminifera (rotaliids), *Amphistegina*, geniculate corallines, victoriellids, and *Neorotalia viennoti* are very rare. LBF tests are slightly abraded. The average proportion of micrite matrix is 49 %. Glaucony grains (~ 0.25 mm in diameter) are common and

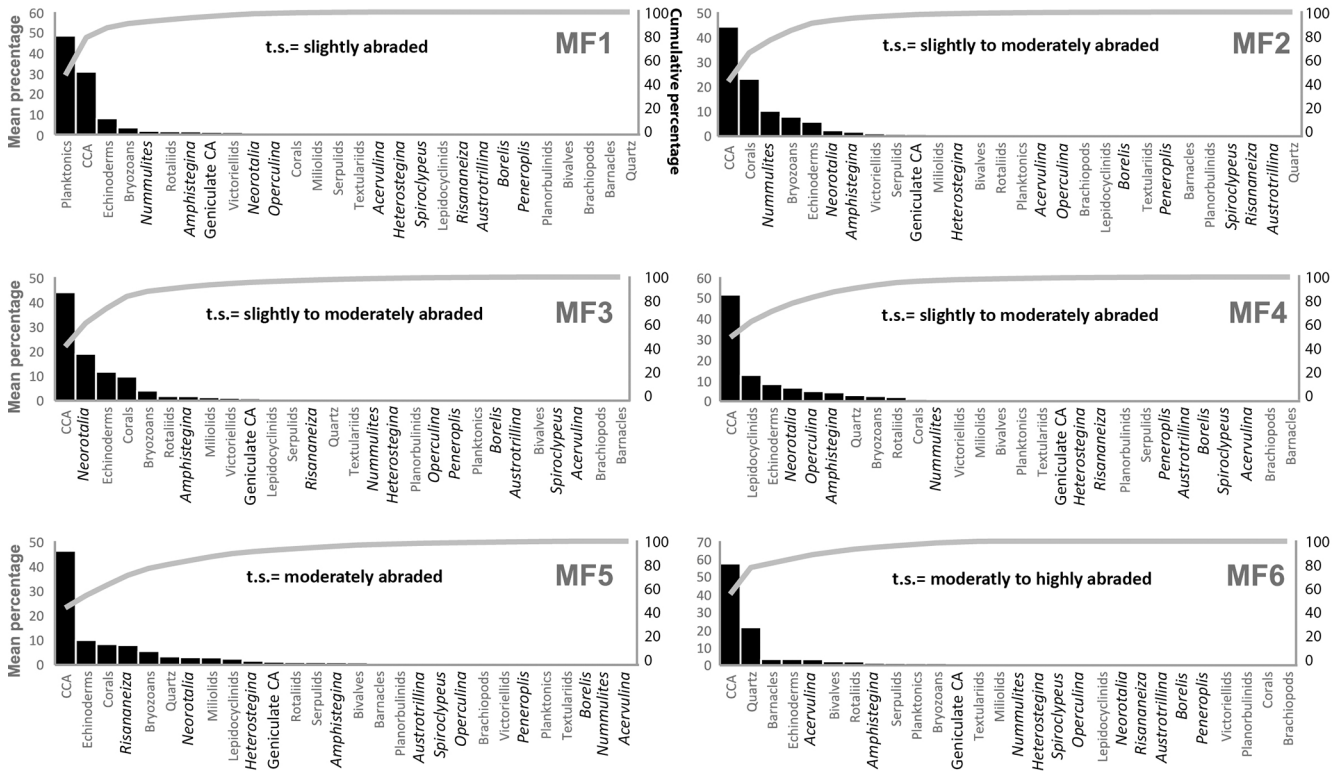

Figure 9. Pareto charts showing the mean relative percentages (*y* axis, left) of all biogenic components (*x* axis) identified in each facies (MF1–MF6). The line represents the cumulative percentage of each component (*y* axis, right). MF1, planktonic foraminiferal wackestone–packstone; MF2, *Nummulites* packstone facies; MF3, *Neorotalia* packstone facies; MF4, lepidocyclinid packstone facies; MF5, *Risananeiza* packstone facies; MF6, bioclastic packstone and quartz facies; t.s., LBF taphonomic signature. Statistic data in Supplement.

occur within foraminiferal chambers. This facies occurs in beds ranging in thickness from 0.1 to 1.8 m in the lower and distal parts of the stratigraphic succession, alternating with MF2 (*Nummulites* packstone facies; Figs. 2, 3–5).

4.3.3 MF2, *Nummulites* packstone

This facies (mean micrite matrix content 37 %; Table S1; Figs. 1, 13a) mostly occurs as massive to well-stratified beds, in packages from 1.5 to 30 m in thickness. It is characterized by *Nummulites* (*N.* cf. *kecskemetii*, *N. vascus*; Fig. 10) associated with common coralline algae and corals. Subordinate components are bryozoans, echinoderms, lepidocyclinids, and *Neorotalia viennoti* (Fig. 12a). Scarce *Amphistegina*, victoriellids, serpulids, geniculate corallines, and small benthic foraminifera (mostly miliolids) also appear together with glauconite grains. *Heterostegina* cf. *assilinoides* (Fig. 10h), bivalve fragments, and planktonic foraminifera are very rare. LBF are from slightly to moderately abraded.

This facies occurs in the lower part of the succession, alternating with MF1 (planktonic foraminiferal wackestone–packstone) and MF3 (Figs. 3–5).

4.3.4 MF3, *Neorotalia* packstone

This packstone (mean micrite matrix content 27 %; Table S1; Figs. 9–13b) is characterized by *Neorotalia viennoti* (Fig. 12a) associated with common coralline algal debris and echinoderms. Subordinate components are corals, bryozoans, *Amphistegina*, smaller benthic foraminifera (rotaliids, miliolids), victoriellids, and geniculate corallines. Lepidocyclinids (*Eulepidina formosoides*, *Nephrolepidina* ex. interc. *morgani* et *praemarginata*; Fig. 11), serpulids, *Risananeiza crassaparies*, textulariids, *Nummulites vascus*, *Heterostegina*, planorbulinids, *Operculina complanata* (Fig. 10g), and quartz grains are very rare. LBF tests show moderately abraded tests. Some beds show a higher degree of sorting, finer grain size, and highly fragmented components (i.e. echinoderms, coralline algae). Sub-angular quartz grains range from 0.25 to 0.5 mm.

This facies occurs in the lower part of the succession in bed packages ranging in thickness from 1 to 16 m, either between

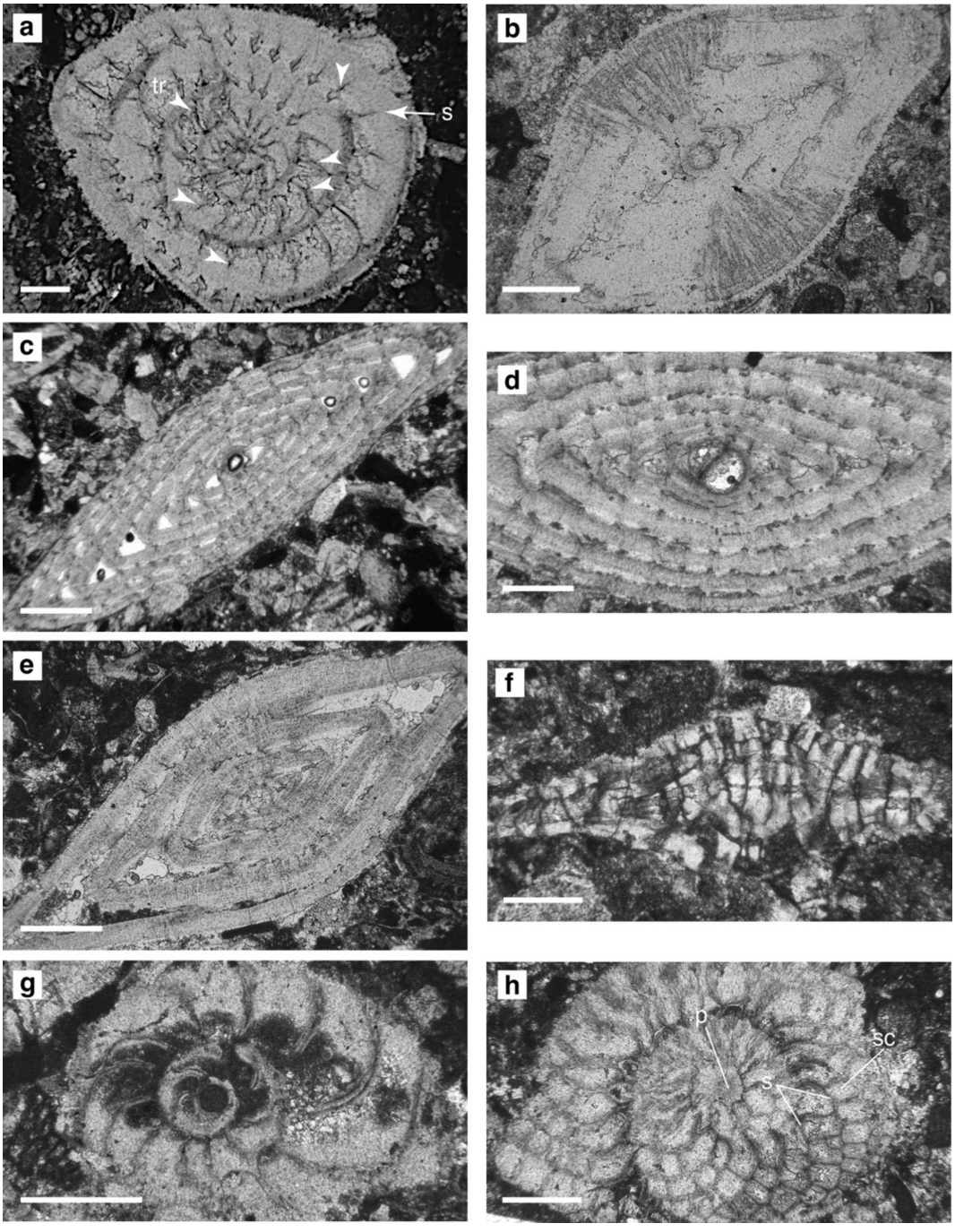

Figure 10. Nummulitid specimens, Sierra de Marmolance. **(a–b)** *Nummulites vascus* Joly and Leymerie, 1848: nearly equatorial section (tr, trabeculae; s, septum) **(a)** and axial section **(b)**, sample M1S6. **(c–d)** *Nummulites fichteli* Michelotti, 1841: axial sections, M2S10, C14. **(e)** *Nummulites* cf. *kecskemetii* Less, 1991: axial section, M1S11. **(f)** *Spiroclypeus* sp.: axial section, M5S8. **(g)** *Operculina complanata* (Defrance, 1822): equatorial section, C16. **(h)** *Heterostegina* cf. *assilinoides* Blackenhorn, 1890 emend. Henson, 1937: equatorial section (p, proloculus; s, septum; sc, stellar chamberlets), M5S8. Scale bar represents 0.4 mm.

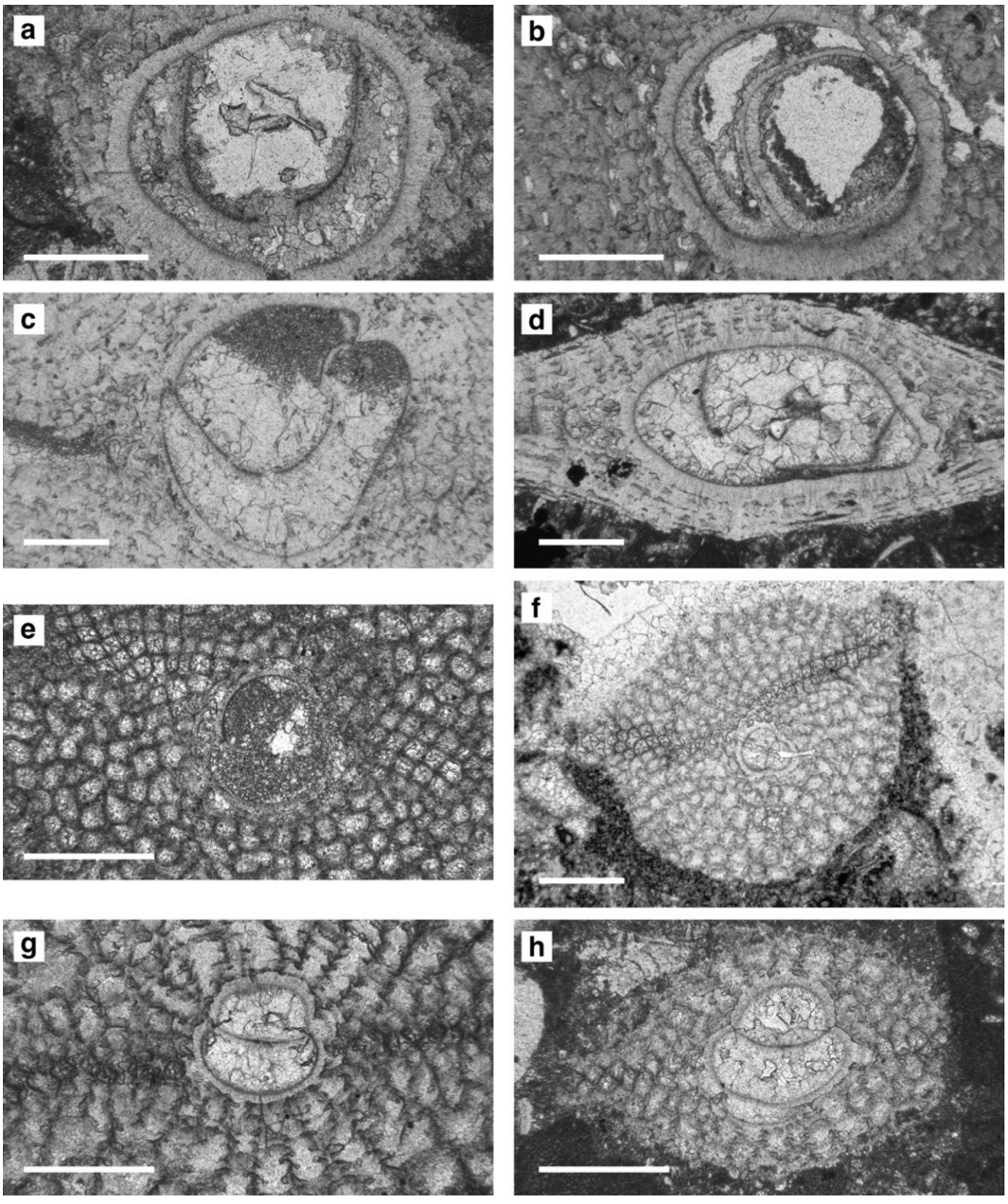

Figure 11. Embryos of megalospheric lepidocyclinid specimens, Sierra de Marmolance. **(a–b)** *Eulepidina formosoides* Douvillé, 1925: sample M1S16, M2S23. **(c–d)** *Eulepidina* ex. interc. *dilatata* (Michelotti, 1861) et *formosoides* Douvillé, 1925: M4S14. **(e–f)** *Nephrolepidina* ex. interc. *morgani* Lemoine and R. Douvillé, 1904 et *praemarginata* R. Douvillé, 1908: M2S1, M2S16. **(g–h)** *Nephrolepidina tournoueri* Lemoine and R. Douvillé, 1904: M5S4, M5S13. Scale bar represents 0.4 mm.

MF2 (*Nummulites* packstone) and MF4 (lepidocyclinid packstone) or alternating with any of them and MF5 (Figs. 3–5).

4.3.5 MF4, lepidocyclinid packstone

This facies is a well-sorted packstone (mean micrite matrix content 32 %; Table S1; Figs. 9, 13c–d) with *Eulepidina* (*E.* ex. interc. *dilatata* et *formosoides*, *E. formosoides*; Fig. 11e–f) and *Nephrolepidina* (*N.* ex. interc. *morgani* et *praemarginata*, *N. tournoueri*; Fig. 11g–h) associated with abundant coralline algal fragments and echinoderms. Subordinate components are *Neorotalia viennoti*, *Operculina complanata* (Fig. 10g), *Amphistegina* sp., quartz grains, bryozoans, and small benthic foraminifera (rotaliids, miliolids). Corals, *Nummulites fichteli* (Fig. 10c–d), victoriellids, miliolids, oyster fragments, PF, textulariids, and geniculate corallines are very rare. Sub-angular quartz grains range in size mostly from 0.25 to 1 mm, occasionally reaching up to

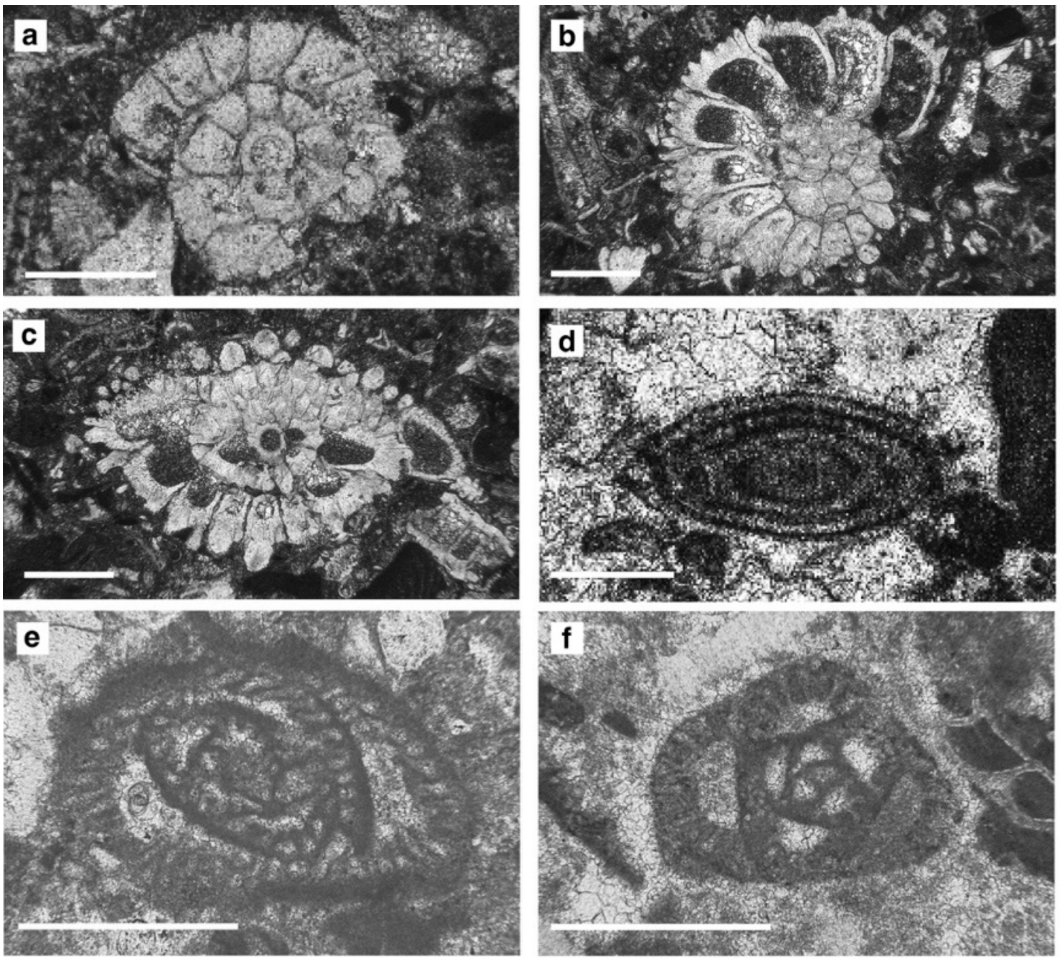

Figure 12. Rotaliid, alveolinoid, and austrotrillinid specimens, Sierra de Marmolance. **(a)** *Neorotalia viennoti* (Greig, 1935): equatorial section, sample M3S13. **(b–c)** *Risananeiza crassaparies* Benedetti and Briguglio, 2012: sub-equatorial section **(b)**, M4S141A; oblique section **(c)**, M4S141A. **(d)** *Borelis inflata* (Adams, 1965): sub-axial section, M5S11_1. **(e)** *Austrotrillina brunni* Marie in Brunn, 1955: tangential section, M4S141. **(f)** *Austrotrillina striata* Todd and Post, 1954: sub-transversal section, M3S13. Scale bar represents 0.4 mm.

2–3 mm. Glauconite grains are present only in a few samples. LBF tests are from slightly to moderately abraded. Highly fragmented and well-sorted lepidocyclinids alternate with well-preserved and unsorted ones.

This facies occurs in bed packages, ranging in thickness from 2 to 35 m, overlying and alternating with MF3 (*Neorotalia* packstone; Figs. 3–5). Small- to medium-scale trough cross-bedding is commonly observed in good exposures of MF4. Cross-bedded intervals alternate or intercalate lenticular to flat beds of the same facies.

4.3.6 MF5, *Risananeiza* packstone

This packstone (mean micrite matrix content 31 %; Table S1; Figs. 9, 13e–g) is characterized by the ornatorotaliid *Risananeiza crassaparies* (Fig. 12b–c) associated with common coralline algal debris, echinoderms, corals, and bryozoans. Subordinate components are quartz grains around 0.25 mm in size, *Neorotalia viennoti*, smaller benthic foraminifera (mostly miliolids), lepidocyclinids (*E.* ex. interc. *dilatata* et *formosoides*, *N.* ex. interc. *morgani* et *premarginata*, *N. tournoueri*), and *Heterostegina* cf. *assilinoides*. Very rare geniculate corallines, serpulids, *Amphistegina* sp., oyster fragments, barnacles, planorbulinids, *Austrotrillina brunni* (Fig. 12e), *A. striata* (Fig. 12f), *Spiroclypeus* sp. (Fig. 10f), *Operculina complanata*, terebratulid brachiopods, victoriellids, *Peneroplis* sp., *Sorites* sp., and *Halimeda* also appear. LBF tests are moderately abraded. Some beds show a higher degree of sorting.

This facies occurs in packages from 15 to 32 m in thickness in the upper part of the succession, overlying and intercalated with MF3 (*Neorotalia* packstone) and underlying MF6 (bioclastic packstone–rudstone with quartz; Figs. 3–5).

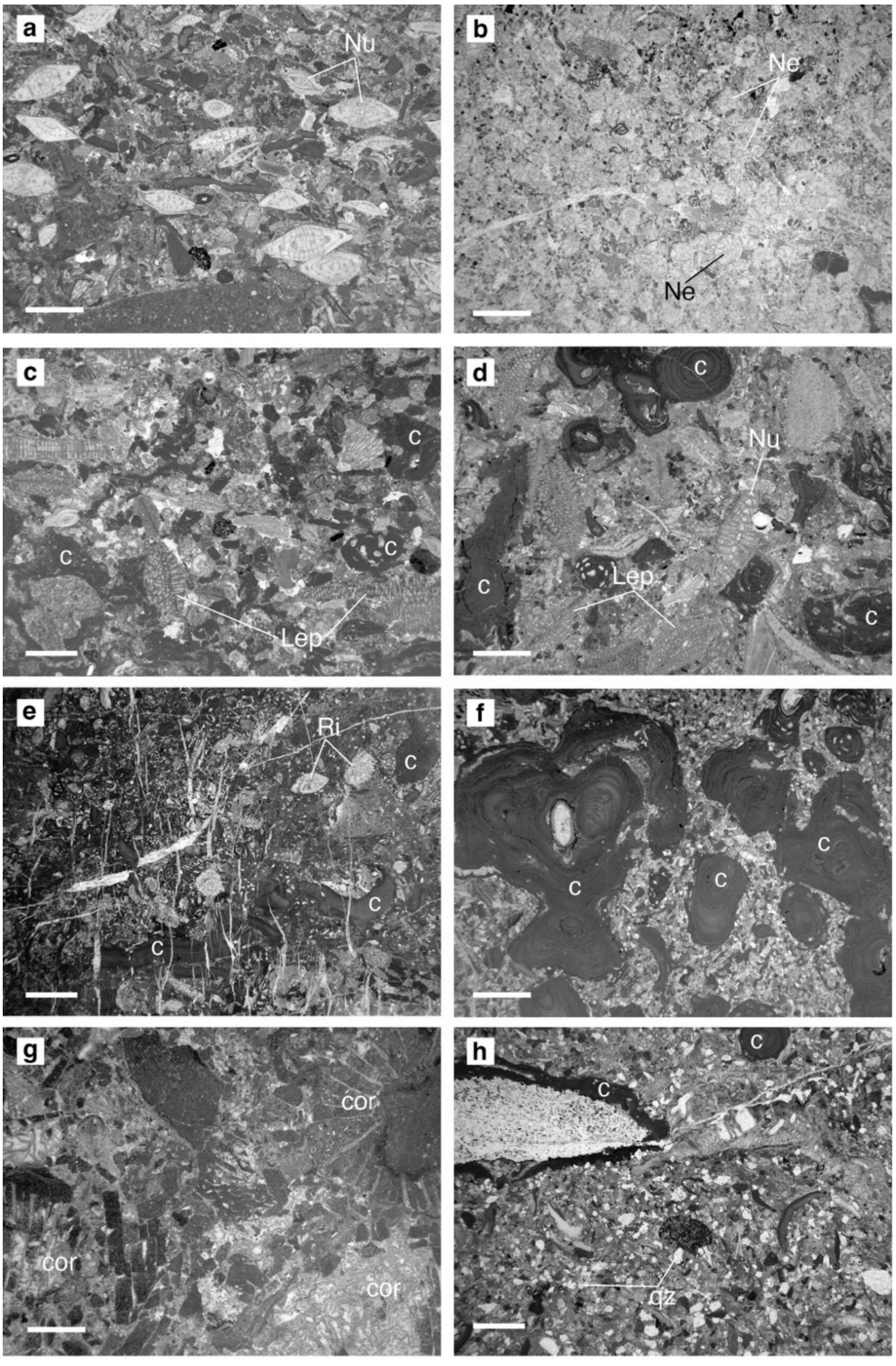

Figure 13. Facies of the Marmolance sedimentary succession, SE Spain. **(a)** *Nummulites* packstone (MF2), sample M1S3. **(b)** *Neorotalia* packstone (MF3), sample M8S25. **(c–d)** Lepidocyclinid packstone (MF4), sample M8S56. **(e–g)** *Risananeiza* packstone (MF5), M5S12. **(h)** Bioclastic packstone and quartz (MF6), sample M5S14. c, corallines; cor, corals; Lep, lepidocyclinids; Ne, *Neorotalia viennoti*; Nu, *Nummulites*; Ri, *Risananeiza crassaparies*; qz, quartz grains. Scale bar represents 2 mm.

4.3.7 MF6, bioclastic packstone–rudstone with quartz

The dominant bioclasts in this facies are coralline algal fragments. Subordinate bioclasts are barnacles, echinoderms, encrusting *Acervulina*, oysters, smaller benthic foraminifera (mostly rotaliids), and *Amphistegina* sp. Serpulids, bryozoans, *Haddonia* sp., PF, and geniculate corallines are very rare (Table S1; Figs. 9, 13h). Sub-angular to sub-rounded quartz/quartzite grains are from poorly sorted (sizes ranging from 0.25 to 40 mm) to well sorted (sizes $\sim$0.5 mm). LBF tests show moderate abrasion, although they are locally highly abraded and fragmented. The average micrite matrix content is 21 % (Table S1).

This facies occurs in the last 5 m of the succession (from 265 m upwards), overlying MF5 (*Risananeiza* packstone; Figs. 3–5).

4.4 Palaeoenvironmental interpretation of facies and depositional model

The outcrop-scale geometry of the Marmolance deposits and the lateral and vertical stratigraphic relationships of lithologies and facies, together with the biogenic components and sedimentary structures, suggest a depositional model of a homoclinal ramp dipping and prograding westwards, with several facies belts following a palaeobathymetric gradient (Fig. 2). The marls with PF were the deepest deposits and changed laterally shorewards (eastwards) to wackestones–packstones with PF (MF1; Fig. 14). This facies formed below the storm-wave base in the outer ramp, as indicated by the well-preserved bioclasts in a micrite-rich matrix with common glauconite grains. Glaucony requires a particular microenvironment at the interface between oxidizing seawater and slightly reducing interstitial waters, which typically occurs at water depths below 50 m (Banerjee et al., 2016). In the deposits older than the Langhian–Serravallian transition (see below and Figs. 3, 14), MF1 changed shoreward to *Nummulites* packstone (MF2). The common occurrence of PF in some beds of this facies with a mud-rich matrix, together with glauconite grains, suggests that MF2 accumulated in the distal middle ramp (Fig. 14). *Neorotalia* packstones (MF3) formed in shallower areas of the middle ramp, with lesser contents of muddy matrix and more fragmented bioclasts, such as coralline algae and echinoderms. The robust and ornamented shells that characterize *Neorotalia* have been interpreted as attachment mechanisms to thrive in high-energy conditions (Hottinger et al., 1991; Beavington-Penney and Racey, 2004), which in this case were probably caused by sporadic storms. These settings where *Neorotalia* thrived are comparable to those described from the Oligocene of the Western Tethys (Reiss and Hottinger, 1984, fig. G.54; Hottinger, 1997; Geel, 2000; Bassi et al., 2007; Bassi and Nebelsick, 2010). Lepidocyclinid packstone (MF4) occurs both as well-sorted cross-bedded intervals and as beds with better preservation of bioclasts (Fig. 13c–d). This suggests this packstone formed in shoals in the inner ramp, with better preservation of the lepidocyclinids that accumulated in the interdune areas (Fig. 14). Lepidocyclinid assemblages have usually been reported from middle-ramp to proximal outer-ramp settings (e.g. Buxton and Pedley, 1989; Beavington-Penney and Racey, 2004; Bover-Arnal et al., 2017; Tomassetti et al., 2018). However, Carozzi et al. (1976), Betzler and Chaproniere (1993), Hottinger (1997), and Simmons (2020) identified a broader depth range for lepidocyclinids from lagoonal to fore-reef settings, in agreement with the inner ramp setting in which lepidocyclinids thrived in Marmolance. Geel (2000) described Oligocene lepidocyclinid deposits from the Prebetic Domain located behind the reef crest, in the near-reef backreef, on shoals with coral thickets, and on the reef front between reef rubble and rhodoliths. In materials accumulated before the Langhian–Serravallian transition, the shallowest recorded sediments comprised lepidocyclinid packstone (Figs. 5, 14). In materials younger than the Langhian–Serravallian transition, no *Nummulites* packstone (MF2) was recorded and MF1 facies changed shorewards to *Neorotalia* packstone (MF3). In addition, shorewards of lepidocyclinid shoals (MF4), the *Risananeiza* packstone (MF5) formed in the shallow inner ramp. This interpretation is supported by the occurrence of porcelaneous LBF (*Austrotrillina*, *Borelis*, and other miliolids; Hottinger, 1997; Simmons, 2020; Bassi et al., 2024) and the robust and ornamented shells typical of *Risananeiza*. This taxon is characterized by thick continuous piles and papillae (Benedetti and Briguglio, 2012; Benedetti et al., 2025), whose function has been interpreted as reducers of total reflection in very shallow settings (Hottinger, 2006). The shallowest facies, which only occurs at top of the limestone succession at the end of the Marmolance ramp progradation, was the bioclastic packstone–rudstone with quartz and quartzites (MF6). The highly fragmented bioclasts, the abundant and well-sorted subrounded siliciclastics, and the presence of large ostreids and balanids suggest proximity to the shoreline in high-energy environments.

Within the general shallowing-upward trend in the vertical succession caused by progradation of ramp deposits, there are cyclical patterns of vertical changes to deeper and shallower facies. The causes of this cyclicity are out of the scope of this work.

4.5 Larger benthic foraminiferal biostratigraphy

The LBF taxa from Sierra de Marmolance are diverse and typical for the western Tethys. They include 18 species belonging to 13 genera: *Amphistegina* sp., *Austrotrillina brunni*, *Austrotrillina striata*, *Borelis inflata*, *Eulepidina* ex. interc. *dilatata* et *formosoides*, *Eulepidina formosoides*, *Heterostegina* cf. *assilinoides*, *Neorotalia viennoti*, *Nephrolepidina* ex. interc. *morgani* et *praemarginata*, *Nephrolepidina tournoueri*, *Nummulites fichteli*, *Nummulites* cf. *kecskemetii*,

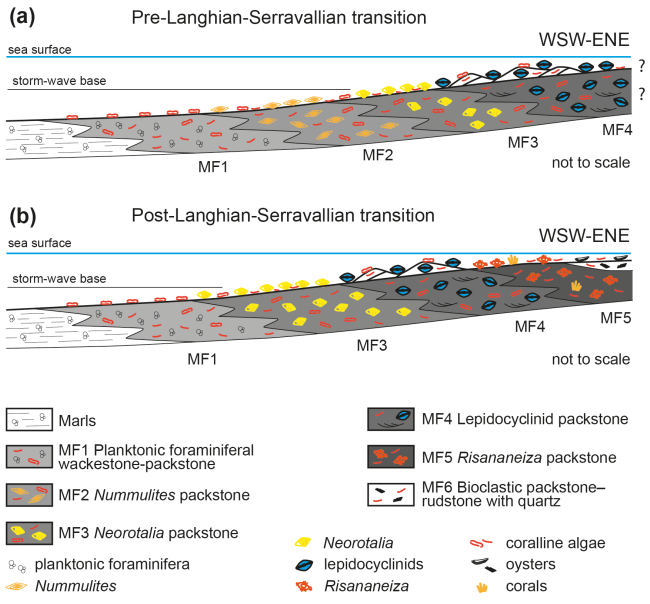

Figure 14. Schematic facies distribution model of the Marmolance carbonate ramp before **(a)** and after **(b)** the Langhian–Serravallian transition.

Nummulites vascus, *Operculina complanata*, *Peneroplis* sp., *Risananeiza crassaparies*, *Sorites* sp., and *Spiroclypeus* sp.

Fragments of Eocene orthophragminids occur in the lower 50 m of Section I at the base of the succession. They are mixed with fragments of coralline algae, corals, echinoids, bryozoans, and scarce *Nummulites vascus*, *Neorotalia viennoti*, and *Amphistegina*.

Section I is characterized by the occurrence of *Nummulites vascus* in almost all samples, whereas *Nummulites* cf. *kecskemetii* is only present at the top of the section (Fig. 3). *Neorotalia viennoti* occurs locally. All these deposits are older than the PF samples indicating the Burdigalian–Langhian transition (Fig. 5).

Nummulites vascus and *N.* cf. *kecskemetii* characterize the first half of Section II, whereas *N. fichteli* occurs in the second half. *Eulepidina formosoides* and *Nephrolepidina* ex. interc. *morgani* et *praemarginata* co-occur from 88 m to the top. There is a single occurrence of *Nephrolepidina tournoueri* at 122 m. Although some beds containing *N. vascus* are older than the planktonic foraminifer samples indicating the Burdigalian–Langhian transition, most *Nummulites* and lepidocyclinid records are Langhian in age. The lepidocyclinids at the top of the section are probably above the Langhian–Serravallian transition (Figs. 3, 5).

Nummulites vascus and *N.* cf. *kecskemetii* occur throughout Section III, whereas *N. fichteli* appears at 68 m from the base. *Eulepidina formosoides* and *Nephrolepidina* ex. interc. *morgani* et *praemarginata* are recorded in a few beds. *Neorotalia viennoti* occurs throughout the section. Porcelaneous LBF are represented by a single record of *Borelis inflata*. In this section, the lower records (lower 25 m) of *Nummulites vascus*, *N.* cf. *kecskemetii*, and *Neorotalia viennoti* are older than the Burdigalian–Langhian transition, but the rest of *Nummulites* occurrences and the lepidocyclinid and *Borelis* records are Langhian in age (Figs. 3, 5).

Section IV shows four distinct intervals of LBF diversity: (1) from the base to ∼ 60 m (6 genera, 10 species), (2) from ∼ 60 to 131 m (5 genera, 6 species), (3) from ∼ 132 m to 153 m where no LBF are recorded, and (4) from ∼ 154 m to the top of the section (10 genera, 11 species). In the lower ∼ 60 m, the LBF assemblages consist of *Nummulites vascus* and *Nummulites* cf. *kecskemetii* with subordinate *Amphistegina* sp. and *Neorotalia viennoti* (Figs. 3, 5). *Nummulites vascus* occurs from the very base of the section. *Nummulites* cf. *kecskemetii* and *N. vascus* occur together 10 to 45 m from the base. The last occurrence of *N. vascus* is at 55 m. From ∼ 60 to 131 m, the only recorded *Nummulites* is *N. fichteli*, and the higher LBF diversity is due to lepidocyclinids (Fig. 4). *N. fichteli* was only found at 60 and 99 m, the latter being the last occurrence of *Nummulites* in the section.

The first occurrence of *Nephrolepidina* ex. interc. *morgani* et *praemarginata* takes place at 53 m from the base, whereas the last occurrence is at 182 m. *Nephrolepidina tournoueri* shows a larger stratigraphic range from 53 to 232 m. *Eulepidina formosoides* occurs from 57 to 115 m. The highest diversity and abundance in lepidocyclinids are recorded between 57 and 115 m, whereas the longest intervals barren in lepidocyclinids are the lower 50 m and from 120 to 178 m.

From 154 m to the top of the section, the LBF are represented by the hyaline perforated *Eulepidina* ex. interc. *dilatata* et *formosoides*, *Heterostegina* cf. *assilinoides*, *Neorotalia viennoti*, *Nephrolepidina tournoueri*, *Operculina complanata*, *Risananeiza crassaparies*, and *Spiroclypeus* sp. and by the larger porcelaneous *Austrotrillina brunni*, *A. striata*, and *Borelis inflata* (Fig. 4).

The first porcelaneous LBF (*Austrotrillina striata*) occurs at 154 m. *Austrotrillina brunni* was locally identified (Figs. 4, 5), and the last record of *B. inflata* is at 261 m. *Risananeiza crassaparies* appears from 168 m to 266 m, nearly coinciding with the porcelaneous LBF occurrences. *Neorotalia viennoti* occurs throughout the section, whereas *Heterostegina* cf. *assilinoides* is limited to the upper part. In Marmolance, the occurrence of *Operculina complanata* nearly corresponds to the interval with the highest lepidocyclinid diversity. *Spiroclypeus* sp. was recorded in a single sample at 246 m.

All records in the lower 105 m of the section can be assigned a Langhian age, whereas all LBF found above are Serravallian or younger (Fig. 5).

Nummulites fichteli, *Operculina complanata*, *Eulepidina formosoides*, *E.* ex. interc. *dilatata* et *formosoides*, *Nephrolepidina* ex. interc. *morgani* et *praemarginata*, and *N. tournoueri* occur in the lower part of Section V (Fig. 4). Undetermined lepidocyclinids and *Neorotalia viennoti* range to the top of the section. *Risananeiza crassaparies*, *Spiroclypeus* sp., and *Borelis inflata* sporadically appear in a few samples. The marls intercalated in the limestones at 23 m

from the base yielded PF assemblages indicative of the Langhian–Serravallian transition (see Sect. 4.4).

5 Discussion

5.1 Autochthony–parautochthony of LBF assemblages

Since the occurrences in Marmolance of several LBF taxa, such as *Eulepidina* ex. interc. *dilatata* et *formosoides*, *Eulepidina formosoides*, *Nephrolepidina* ex. interc. *morgani* et *praemarginata*, *Nephrolepidina tournoueri*, *Nummulites fichteli*, *Nummulites* cf. *kecskemetii*, *Nummulites vascus*, *Risananeiza crassaparies*, and *Spiroclypeus* sp., are much younger than previously known, the immediate question that arises is whether the recorded LBF are reworked from older deposits in the region and incorporated in strata younger than the marly beds with planktonic foraminifera marking the Burdigalian–Langhian transition and the Langhian–Serravallian boundary. Two evidence lines, however, point to the autochthonous–parautochthonous character of the LBF assemblages. The most significant one is the occurrence of facies characterized by distinct LBF assemblages for generally long section intervals: *Nummulites* packstone, *Neorotalia* packstone, lepidocyclinid packstone, *Risananeiza* packstone. These facies replace each other in vertical successions with gradual component changes in some cases, but there is a general absence of mixing up of LBF from several facies in the same beds. This means that LBF are recorded in deposits formed in different palaeoenvironments (facies belts), each one characterized by a distinct biotic composition, which, in addition, has been quantitatively defined and has statistical significance. Therefore, the LBF components are autochthonous in the corresponding facies belt or parautochthonous in the case that they underwent a certain degree of remobilization from their life position. The latter is clearly the case of lepidocyclinids occurring in the cross-bedded limestones of the lepidocyclinid packstone facies, which were incorporated in submarine dunes in the inner ramp. The distribution of LBF species in particular bed sets in Marmolance was already pointed out by Foucault (1971), suggesting that this stratigraphic organization was due to ecological factors.

A second line of evidence is the bed-scale occurrence of LBF and their preservation. In most cases, they occur in flat-bedded wackestone to packstone with no sedimentary structures characteristic of coarse-grained sediment gravity flows that could point to allochthonous sediment provenance. In the case of LBF in cross-bedded packstone, the obvious remobilization of particles took place inside the ramp, in submarine dunes fed from bioclasts mainly produced within a single facies belt, as suggested by the singularity of their LBF composition dominated by lepidocyclinids. Except in this latter case, the preservation of LBF tests indicated limited to no transport, reinforcing the autochthonous–parautochthonous character of their assemblages.

In contrast to these general features in the study sections, in the lowest 50 m of Section I, fragmented orthophragminids occur mixed with other bioclasts in packstone beds immediately below and above marls, suggesting they are reworked from Eocene rocks and incorporated in sediment gravity flow deposits.

5.2 Chronostratigraphic distribution of larger benthic foraminifera

Although previous biostratigraphic zonations limited *Spiroclypeus* and *Nummulites* to the Oligocene (Cahuzac and Poignant, 1997) and *Eulepidina* and *Nephrolepidina* to the Early Miocene in the western Mediterranean (Hottinger, 1977; Less and Özcan, 2008; BouDagher-Fadel and Price, 2014; Serra-Kiel et al., 2016; Benedetti and Schiavinotto, 2023), these genera reached the Middle Miocene in the Marmolance succession. Considering the SBZ of Cahuzac and Poignant (1997), the LBF species identified in the Marmolance sections should have indicated a Rupelian–Burdigalian age. According to these authors, *Nummulites fichteli*, *N. vascus*, *Eulepidina formosoides*, *E. dilatata*, and *Nephrolepidina praemarginata* characterize the Oligocene, whereas the latemost occurrence of *Nephrolepidina morgani* and the whole occurrence of *N. tournoueri* would have marked the Aquitanian and the Burdigalian, respectively. In Marmolance, however, *Nephrolepidina tournoueri* co-occurs with *Nephrolepidina* ex. interc. *morgani* et *praemarginata*, *Eulepidina* ex. interc. *dilatata* et *formosoides*, and *N. fichteli* (Fig. 15).

Among these genera, only *Nummulites* is extant, living in the modern central Indo-Pacific (Langer and Hottinger, 2000; Hohenegger, 2000). In Marmolance, *Nummulites vascus* and *N.* cf. *kecskemetii* occur below and above the Burdigalian–Langhian transition but disappear below the Langhian–Serravallian boundary beds. In contrast, *Nummulites fichteli* is only recorded above the Burdigalian–Langhian transition.

The classically assumed LAD of *Spiroclypeus* at the end of the Chattian (Cahuzac and Poignant, 1997) and those of *Eulepidina*, *Nephrolepidina*, and *Miogypsina* at the end of the Burdigalian (Drooger and Laagland, 1986; Drooger, 1993; Cahuzac and Poignant, 1997; Özcan and Less, 2009; Özcan et al., 2010) were based on indirect correlations not straightforwardly supported by stratigraphically related PF assemblages. The LAD of *Spiroclypeus* at the Oligocene–Miocene boundary was already questioned by the Lower Miocene records of *Spiroclypeus anghiarensis*, *S. blanckenhorni*, and *S. tidoenganensis* from the Western Tethys (Henson, 1937; Hottinger, 1977; Less and Özcan, 2008; Özcan et al., 2009b; BouDagher-Fadel and Price, 2014; Serra-Kiel et al., 2016; Ferràndez-Cañadell and Bover-Arnal, 2017). Although *Spiroclypeus anghiarensis* was taxonomically re-assessed as *Tansinhokella anghiarensis* (Banner and Hodgkinson, 1991), no morphological criteria are likely clear to separate the late Eocene *Heterostegina* (*Vlerkina*), *Tansin-*

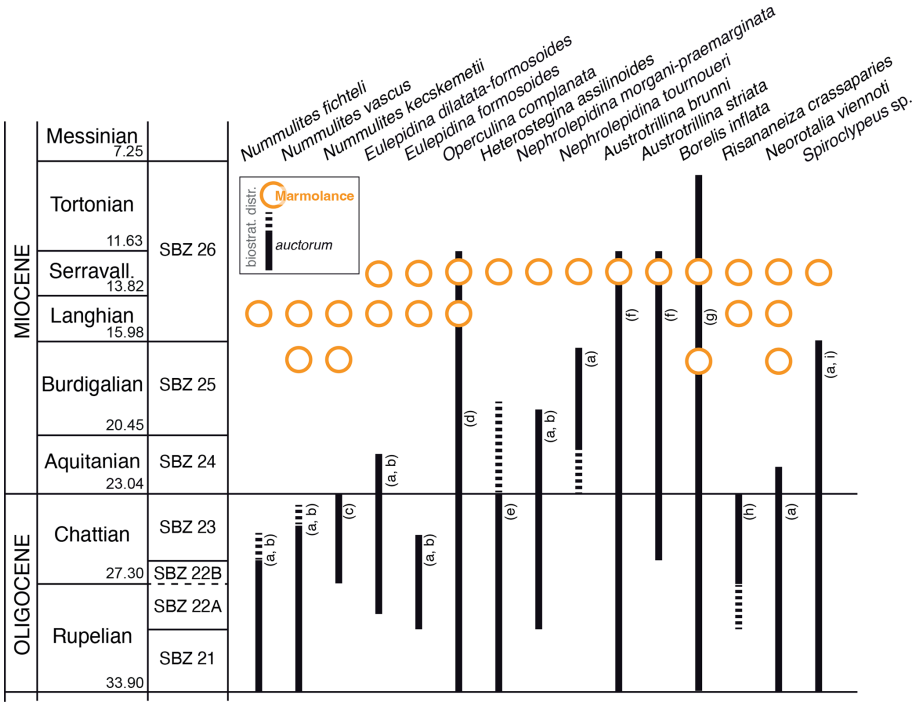

Figure 15. Stratigraphic distributions of the LBF species identified in Marmolance compared with those reported in the literature (*auctorum*). Dashed lines point to possible occurrence in that stratigraphic interval. **(a)** Cahuzac and Poignant (1997), Ferràndez-Cañadell and Bover-Arnal (2017); **(b)** Drooger and Laagland (1986), Drooger (1993); **(c)** Less et al. (2011), Ferràndez-Cañadell and Bover-Arnal (2017); **(d)** Hottinger (1977), Cahuzac and Poignant (1997), Ferràndez-Cañadell and Bover-Arnal (2017); **(e)** Hottinger (1977), Cahuzac and Poignant (1997), Özcan et al. (2009a), Ferràndez-Cañadell and Bover-Arnal (2017), Benedetti et al. (2017); **(f)** Bassi et al. (2021a); **(g)** Bassi et al. (2021b); **(h)** Benedetti and Briguglio (2012), Ferràndez-Cañadell and Bover-Arnal (2017), Benedetti et al. (2025); **(i)** Less and Özcan (2008), Özcan and Less (2009), Serra-Kiel et al. (2016). Timescale after Cohen et al. (2025).

hokella, and *Spiroclypeus* from the later Oligocene forms (Lunt and Renema, 2014). In Marmolance, the single record of *Spiroclypeus* is younger than the Langhian–Serravallian transition marked by PF (Figs. 5, 15).

Cahuzac and Poignant (1997) established the LAD of *Eulepidina dilatata* in the Oligocene–Miocene boundary, although previous reports indicated that the species likely crossed that boundary (Sirotti, 1982). Özcan and Less (2009) stated that the stratigraphic age of some *Eulepidina* records cannot be confidently demonstrated due to the absence of associated age-diagnostic taxa (e.g. PF). Up to now, the last occurrence of *Eulepidina* was found in Aquitanian deposits from Greece (Wielandt-Schuster, 2004). The Western Tethyan *Nephrolepidina* species circumscriptions are based on two morphological parameters: the number of adauxiliary chamberlets and the degree of embracement of the protoconch by the deuteroconch (*A* parameter; van der Vlerk, 1959; de Mulder, 1975; Drooger, 1993). The increasing values of these parameters define the chronospecies succession *Nephrolepidina praemarginata*/*N. morgani*/*N. tournoueri* (de Mulder, 1975). This *Nephrolepidina* species succession applied by many authors (e.g. Sirotti, 1982; Özcan et al., 2009a, b; Benedetti and Pignatti, 2013) was initially based on the schemes of de Mulder (1975) and later Cahuzac and Poignant (1997). The latest species, *N. tournoueri*, supposedly disappears in the Burdigalian (SBZ 25; Özcan and Less, 2009; Benedetti and Schiavinotto, 2023), and a possible biostratigraphic overlap with *N. morgani* was not excluded (Özcan and Less, 2009, p. 24; Fig. 15). The single illustrated record of *Lepidocyclina (Nephrolepidina) aquitaniae* Silvestri, 1912 from the Serravallian of an unknown locality in Spain (BouDagher-Fadel and Price, 2010) needs further systematic and stratigraphic assessment. In Marmolance, *Eulepidina* ex. interc. *dilatata* et *formosoides*, *E. formosoides*, *Nephrolepidina* ex. interc. *morgani* et *praemarginata*, and *N. tournourei* occur in beds above both the Burdigalian–Langhian and Langhian–Serravallian transitions.

Up to now, *Risananeiza* has only been found in Oligocene rocks (Benedetti and Briguglio, 2012; Benedetti et al., 2025) and *Neorotalia viennoti* was assumed to disappear in the Early Miocene (Cahuzac and Poignant, 1997). In Marmolance, however, the former occurs well above the Langhian–Serravallian transition and the latter is commonly found both in Langhian and Serravallian beds and in the limestones below the Burdigalian–Langhian transition (Fig. 15).

6 Conclusions

Planktonic foraminiferal assemblages in the marls, underlying and laterally changing to bioclastic limestones in the Sierra de Marmolance (External Zones, Betic Cordillera, SE Spain), indicate a late Burdigalian–early Serravallian age for the succession. Outcrop-scale geometry, stratigraphic patterns, facies distribution, and biogenic components show that the Marmolance limestones formed on a westward-prograding carbonate ramp. In the Burdigalian–Langhian interval, planktonic foraminiferal packstone and marls constitute the outer-ramp deposits, which pass shorewards into the distal middle-ramp *Nummulites* packstone; in the proximal middle ramp, *Neorotalia* grew under sporadic high-energy conditions. Distal inner-ramp shoals with lepidocyclinids are the shallowest deposits in this interval. In the Serravallian, no *Nummulites* packstone occurs; the ornatorotaliid *Risananeiza* with porcelaneous LBF are the main components in packstone shorewards of the lepidocyclinid shoals; mixed siliciclastics and carbonates with large oysters and balanids accumulated in the shallowest settings.

Altogether, 18 LBF species were identified in the Marmolance succession: *Amphistegina* sp.; *Austrotrillina brunni* Marie in Brunn et al., 1955; *Austrotrillina striata* Todd and Post, 1954; *Borelis inflata* (Adams, 1965); *Eulepidina* ex. interc. *dilatata* (Michelotti, 1861) et *formosoides* Douvillé, 1925; *Eulepidina formosoides* Douvillé, 1925; *Heterostegina* cf. *assilinoides* Blackenhorn, 1890 emend. Henson, 1937; *Neorotalia viennoti* (Greig, 1935); *Nephrolepidina* ex. interc. *morgani* Lemoine and R. Douvillé, 1904 et *praemarginata* R. Douvillé, 1908; *Nephrolepidina tournoueri* Lemoine and Douvillé, 1904; *Nummulites fichteli* Michelotti, 1841; *Nummulites* cf. *kecskemetii* Less, 1991; *Nummulites vascus* Joly and Leymerie, 1848; *Operculina complanata* (Defrance, 1822); *Peneroplis* sp.; *Risananeiza crassaparies* Benedetti and Briguglio, 2012; *Sorites* sp.; and *Spiroclypeus* sp. Before the present study, 7 of these species (*Eulepidina dilatata*, *E. formosoides*, *Nephrolepidina praemarginata*, *Nummulites fichteli*, *N. vascus*, *N. kecskemetii*, *Risananeiza crassaparies*) were considered exclusively Oligocene taxa, whereas 4 species (*Nephrolepidina morgani*, *N. tournoueri*, *Neorotalia viennoti*, *Spiroclypeus* sp.) were supposed to disappear in the Early Miocene.

Nummulites vascus and *N.* cf. *kecskemetii* occur in Burdigalian and Langhian strata, whereas *N. fichteli* only appears in Langhian beds. The chronostratigraphic range of *Eulepidina dilatata*, *E. formosoides*, *Nephrolepidina morgani*, *N. praemarginata*, *N. tournoueri*, *Neorotalia viennoti*, *Risananeiza crassaparies*, and *Spiroclypeus* sp. extends at least to the Serravallian. The record of *Nummulites* species in the Langhian of SE Spain partly fills the stratigraphic gap of this genus thought to be extinct at the end of the Oligocene but still living in modern Indo-Pacific areas. The occurrence of lepidocyclinids in the Serravallian of Marmolance points out their long persistence in the Western Tethys.

In addition to the chronostratigraphic implications, the results of this study substantially change the understanding of the evolutionary history and palaeobiogeographical patterns of LBF. Our findings significantly modify the current ideas about Neogene LBF biodiversity in the Mediterranean area.

7 Taxonomic remarks

Nummulites species are characterized by small, flattened tests (*N. fichteli*, *N.* cf. *kecskemetii*) and small lenticular tests (*N. vascus*) (Fig. 10a–e). Specimens of *Nummulites vascus* show thick lenticular tests and a roughly defined central boss. The test diameter (D) ranges between 1.9 and 4.8 mm (mean 2.7 mm). The proloculus (P) is $\sim 160\,\mu m$ in mean diameter (ranging from 110 to 235 µm), and the chamber length in the third whorl ranges from 140 to 340 µm (mean 204 µm). *Nummulites* cf. *kecskemetii* is characterized by a flattened test with a mean diameter of 2.6 mm. The small protoconch is 70–100 µm in diameter (mean 90 µm), and the chamber length in the third whorl ranges from 200 to 380 µm (mean 270 µm). Specimens of *Nummulites fichteli* are typically flat and biconvex in shape. The test diameter ($D = 2.2$–4.8 mm; mean 3.4 mm), the proloculus size ($P = 115$–$420\,\mu m$; mean 234 µm), and the chamber length in the third whorl ($L = 105$–$190\,\mu m$; mean 145 µm) were measured in 14 axial sections of megalospheric specimens.

Nephrolepidina ex. interc. *morgani* et *praemarginata* is represented by 18 sub-equatorial sections (A parameter = 40–45, mean 40; diameter of the protoconch $P = 155$–$310\,\mu m$, mean 228 µm; and deuteroconch $D = 200$–$400\,\mu m$, mean 300 µm) (Fig. 11e–f). For comparison, see de Mulder (1975, pl. 3, fig. 7), Özcan et al. (2010, pl. 2, figs. 20–26), Ghafor (2015, figs. 11. 7–10), Less et al. (2018, fig. 14. 7–12), Parente and Less (2019, fig. 20a–e), Benedetti and Pignatti (2013), and Benedetti (2014). *Nephrolepidina tournoueri* was identified in 6 sub-equatorial sections (A parameter = 45–50, mean 46; diameter of the protoconch $P = 225$–$470\,\mu m$, mean 317 µm; and deuteroconch $D = 380$–$575\,\mu m$, mean 455 µm) (Fig. 11g–h). *Eulepidina formosoides* was identified by means of deuteroconch ($D_{mean} = 996\,\mu m$) and protoconch ($P_{mean} = 697\,\mu m$) sizes in 4 equatorial sections (Fig. 11a–b). In sub-oblique axial sections, A parameter = 60, the protoconch diameter is 430–980 µm ($P_{mean} = 614\,\mu m$) and the deuteroconch width is 600–1330 µm ($D_{mean} = 914\,\mu m$).

In sample M5-S4 (231 m from the base of Section IV), a single lepidocyclinid specimen shows the diameter of the protoconch ($P = 960\,\mu m$) and deuteroconch ($D = 1260\,\mu m$) comparable to those of *Eulepidina dilatata* but with an unusually small A parameter ($A = 60$), typical of *E. formosoides* ($A_{mean} < 83$; e.g. Özcan et al., 2009a, 2010). This Marmolance specimen therefore has intermediate characteristics between *Eulepidina dilatata* and *E. formosoides*, being closer to the former. Because *Eulepidina dilatata*

and *E. formosoides* are two successive and phylogenetically linked species belonging to the same lineage (van Heck and Drooger, 1984; Özcan et al., 2010), the specimen was ascribed to *E.* ex. interc. *dilatata* et *formosoides* (Fig. 11c–d).

Heterostegina cf. *assilinoides* show a protoconch (P) $\sim$ 120 µm in diameter, measured from axial and nearly oblique sections. The sub-axial sections of the specimens show thick pillars throughout the inflated umbonal region (Fig. 10h). Internal stellate chambers surrounding the protoconch and the deuteroconch occur in sub-equatorial sections; see for comparison Less et al. (2008, fig. 18), Boukhary et al. (2008, pl. 3, fig. 11), Özcan et al. (2009a, figs. 20.4, 20.10), Ferràndez-Cañadell and Bover-Arnal (2017, fig. 8A–F), and Less et al. (2018, fig. 10).

Sub-axial and oblique sections of *Neorotalia viennoti* show a trochospiral test with a thick ventral pile that leads to an asymmetrical outline in axial section (Fig. 12a). The proloculus is $\sim$ 110 µm in diameter (e.g. Bassi et al., 2007; BouDagher-Fadel and Price, 2013; Hottinger, 2014; Ferràndez-Cañadell and Bover-Arnal, 2017).

Sub-equatorial sections of *Operculina* with a proloculus diameter (P) ranging between 95 and 135 µm (mean 111 µm) were ascribed to *Operculina complanata*, corresponding to *Planoperculina complanata* (Defrance, 1822) in Hottinger (1977, p. 101; see also Less, 1991, and Less et al., 2011). The specimens show a rapidly opening spire, with few whorls and folded septa (Fig. 10g).

Risananeiza crassaparies is characterized by a hemispherical to flattened shell, ranging in diameter from 1 to 1.80 mm, with a test thickness ranging from 70 to 95 µm (Fig. 12b–c). The subspherical proloculus ranges in size from 74–182 µm (mean 12 µm), a little larger than the deuteroconch, followed by spirally arranged chambers. The chamber height/chamber ratio width is $\sim$ 1.6 (Benedetti and Briguglio, 2012). Shells show thick pillars from the umbilical region and the intraseptal canal system developed for each chamber. Very rare B-forms were found.

Sub-axial sections of rare nummulitid specimens showing spiral chambers subdivided in secondary chamberlets by secondary septa and lateral chamberlets arranged symmetrically on both sides of the spiral were ascribed to *Spiroclypeus* sp. The examined specimens do not show diagnostic characters for species identification.

Below is a taxonomic list of LBF species mentioned in the text and figures, listed in alphabetical order.

Austrotrillina brunni Marie in Brunn et al., 1955

Austrotrillina striata Todd and Post, 1954

Borelis inflata (Adams, 1965)

Eulepidina ex. interc. *dilatata* (Michelotti, 1861) et *formosoides* Douvillé, 1925

Eulepidina formosoides Douvillé, 1925

Heterostegina assilinoides Blackenhorn, 1890 emend. Henson, 1937

Neorotalia viennoti (Greig, 1935)

Nephrolepidina ex. interc. *morgani* Lemoine and R. Douvillé, 1904 et *praemarginata* R. Douvillé, 1908

Nephrolepidina tournoueri Lemoine and R. Douvillé, 1904

Nummulites kecskemetii Less, 1991

Nummulites vascus Joly and Leymerie, 1848

Nummulites fichteli Michelotti, 1841

Operculina complanata (Defrance, 1822)

Risananeiza crassaparies Benedetti and Briguglio, 2012

Data availability. Microscope slides are stored in the collection of the Departamento de Estratigrafía y Paleontología, Universidad de Granada. All data sets discussed in the present work are available in the Supplement.

Supplement. The supplement related to this article is available online at https://doi.org/10.5194/jm-44-573-2025-supplement.

Author contributions. All authors performed input for methodology, investigation, formal analysis, and data curation. All authors interpreted the results and wrote and edited the article. JCB designed the research. JA, DB, and JCB provided funding acquisition.

Competing interests. The contact author has declared that none of the authors has any competing interests.

Disclaimer. Publisher's note: Copernicus Publications remains neutral with regard to jurisdictional claims made in the text, published maps, institutional affiliations, or any other geographical representation in this paper. While Copernicus Publications makes every effort to include appropriate place names, the final responsibility lies with the authors. Views expressed in the text are those of the authors and do not necessarily reflect the views of the publisher.

Acknowledgements. This study was supported by the local research fund of the University of Ferrara (FAR 2020–2023). This paper is a scientific contribution of the Project MIUR–Dipartimenti di Eccellenza 2018–2022, of the research project PID2022-142806NB-100 funded by MICIU/AEI/10.13039/501100011033 and by ERDF "A Way of Making Europe", and of the Research Group RNM 190 of Junta de Andalucía. Reviews and comments by the editor and two anonymous reviewers are much appreciated.

Financial support. This research has been supported by the Università degli Studi di Ferrara (grant no. FAR 2020–2023); the Ministero dell'Istruzione, dell'Università e della Ricerca (grant no. Dipartimenti di Eccellenza 2018–2022); the Ministerio de Ciencia e Innovación (grant no. MICIU/AEI/10.13039/501100011033 and by ERDF "A Way of Making Europe"); and the Consejería de Conocimiento, Investigación y Universidad, Junta de Andalucía (grant no. RNM 190).

Review statement. This paper was edited by Laia Alegret and reviewed by two anonymous referees.

References

Adams, C. G.: The Foraminifera and stratigraphy of the Melinau Limestone, Sarawak, and its importance in Tertiary correlation, Q. J. Geol. Soc. Lond., 121, 283–338, https://doi.org/10.1144/gsjgs.121.1.0283, 1965.

Adams, C. G., Gentry, A. W., and Whybrow, P. J.: Dating the terminal Tethyan event, Utrecht Micropaleontol. Bull., 30, 273–298, 1983.

Al-Qayim, B., Ibrahim, A., and Kharajiany, S.: Microfacis and sequence stratigraphy of the Oligocene–Miocene sequence at Golan Mountian, Kurdistan, Iraq, Carbonates and Evaporites, 31, 259–276, https://doi.org/10.1007/s13146-015-0262-5, 2016.

Aze, T., Ezard, T. H. G., Purvis, A., Coxall, H. K., Steward, D. R. M., Wade, B. S, and Pearson, P. N.: A phylogeny of Cenozoic macroperforate planktonic foraminifera from fossil data, Biol. Rev., 86, 900–927, https://doi.org/10.1111/j.1469-185X.2011.00178.x, 2011.

Banerjee, S., Bansal, U., and Thorat, A. V.: A review on palaeogeographic implications and temporal variation in glaucony composition, J. Palaeogeogr., 5, 43–71, https://doi.org/10.1016/j.jop.2015.12.001, 2016.

Banner, F. T. and Hodgkinson, L. R.: A revision of the foraminiferal subfamily Heterostegininae, Rev. Españ. Micropaleontol., 23, 101–140, 1991.

Bassi, D. and Nebelsick, J. H.: Components, facies and ramps: redefining Upper Oligocene shallow water carbonates using coralline red algae and larger foraminifera (Venetian area, northeast Italy), Palaeogeogr. Palaeoclimatol. Palaeoecol., 295, 258–280, https://doi.org/10.1016/j.palaeo.2010.06.003, 2010.

Bassi, D., Woelkerling, W. J., and Nebelsick, J. H.: Taxonomic and biostratigraphical re-assessments of *Subterraniphyllum* Elliott (Corallinales, Rhodophyta), Palaeontology, 43, 405–425, https://doi.org/10.1111/j.0031-0239.2000.00133.x, 2000.

Bassi, D., Hottinger, L., and Nebelsick, J. H.: Larger Foraminifera from the upper Oligocene of the Venetian area, north-east Italy, Palaeontology, 50, 845–868, https://doi.org/10.1111/j.1475-4983.2007.00677.x, 2007.

Bassi, D., Nebelsick, J. H., Puga-Bernabéu, Á., and Luciani, V.: Middle Eocene *Nummulites* and their offshore redeposition: a case study from Middle Eocene of the Venetian area, northeastern Italy, Sediment. Geol., 297, 1–15, https://doi.org/10.1016/j.sedgeo.2013.08.012, 2013.

Bassi, D., Braga, J. C., Di Domenico, G., Pignatti, J., Abramovich, S., Hallock, P., Könen, J., Kovács, Z., Langer, M. R., Pavia, G., and Iryu, Y.: Palaeobiogeography and evolutionary patterns of the larger foraminifer *Borelis* de Montfort (Borelidae), Pap. Palaeontol., 7, 377–403, https://doi.org/10.1002/spp2.1273, 2021a.

Bassi, D., Aftabuzzaman, Md., Bolivar-Feriche, M., Braga, J. C., Aguirre, J., Renema, W., Takayanagi, H., and Iryu, Y.: Biostratigraphical and palaeobiogeographical patterns of the larger porcelaneous foraminifer *Austrotrillina* Parr, 1942, Mar. Micropal., 169, 102058, https://doi.org/10.1016/j.marmicro.2021.102058, 2021b.

Bassi, D., Braga, J. C., Pignatti, J., Fujita, K., Nebelsick, J. H., Renema, W., and Iryu, Y.: Porcelaneous larger foraminiferal responses to Oligocene–Miocene global changes, Palaeogeogr. Palaeoclimatol. Palaeoecol., 634, 111916, https://doi.org/10.1016/j.palaeo.2023.111916, 2024.

Beavington-Penney, S. J.: Analysis of the effects of abrasion on the test of *Palaeonummulites venosus*: implications for the origin of nummulithoclastic sediments, Palaios, 19, 143–155, https://doi.org/10.1669/0883-1351(2004)019<0143:AOTEOA>2.0.CO;2, 2004.

Beavington-Penney, S. J. and Racey, A.: Ecology of extant nummulitids and other larger benthic foraminifera: applications in palaeoenvironmental analysis, Earth-Sci. Rev., 67, 219–265, https://doi.org/10.1016/j.earscirev.2004.02.005, 2004.

Benedetti, A.: Spiral growth in *Nephrolepidina*: evidence of "golden selection", Paleobiology, 40, 151–161, https://doi.org/10.1666/12057, 2014.

Benedetti, A. and Briguglio, A.: *Risananeiza crassaparies* n. sp. from the upper Chattian of Porto Badisco (southern Apulia, Italy), Boll. Soc. Paleontol. It., 51, 167–176, https://doi.org/10.1666/12057, 2012.

Benedetti, A. and Pignatti, J.: Conflicting evolutionary and biostratigraphical trends in *Nephrolepidina praemarginata* (Douvillé, 1908) (Foraminiferida), Hist. Biol., 25, 363–383, https://doi.org/10.1080/08912963.2012.713949, 2013.

Benedetti, A. and Schiavinotto, F.: Evolutionary trends in the Mediterranean *Nephrolepidina*: new chronosubspecies and biostratigraphic constraints, Hist. Biol., 35, 518–536, https://doi.org/10.1080/08912963.2022.2054711, 2023.

Benedetti, A., Less, G., Parente, M., Pignatti, J., Cahuzac, B., Torres-Silva, A. I., and Buhl, D.: *Heterostegina matteuccii* sp. nov. (Foraminiferida: Nummulitidae) from the Lower Oligocene of Sicily and Aquitaine: a possible transatlantic immigrant, J. Syst. Palaeont., 16, 87–110, https://doi.org/10.1080/14772019.2016.1272009, 2017.

Benedetti, A., Briguglio, A., Consorti, L., and Papazzoni, C. A.: Paleoecological and paleoenvironmental insights from Ornatorotaliidae (larger foraminifera), Mar. Micropal., 194, 102423, https://doi.org/10.1016/j.marmicro.2024.102423, 2025.

Betzler, C. and Chaproniere, G. C. H.: Paleogene and Neogene larger foraminifers from the Queensland Plateau: biostratigraphy and environmental significance, in: Proceedings of the Ocean Drilling Program, Scientific Results 133, edited by: College Station, TX (Ocean Drilling Program), 51–66, https://doi.org/10.2973/odp.proc.sr.133.210.1993, 1993.

Betzler, C. and Schmitz, S.: First record of *Borelis melo* and *Dendritina* sp. in the Messinian of SE Spain (Cabo de Gata, Province Almeria), PalZ, 71, 211–216, https://doi.org/10.1007/BF02988489, 1997.

Blow, W. H.: Transatlantic correlation of Miocene sediments, Micropaleontology, 3, 77–79, 1957.

Blow, W. H.: Late Middle Eocene to recent planktonic foraminiferal biostratigraphy, Proc. 1st Int. Plankt. Conf. Geneva, 1, 199–422, https://doi.org/10.1163/9789004616455_018, 1969.

Bolli, H. M. and Saunders, J. B.: Oligocene to Holocene Low Latitude Planktonic Foraminifera, in: Plankton Stratigraphy, edited by: Bolli, H. M., Saunders, J. B., and Perch-Nielsen, K., Cambridge University Press, Cambridge, 155–257, 1985.

BouDagher-Fadel, M. K.: Evolution and geological significance of larger benthic foraminifera, 2nd edn., University College London Press, London, https://doi.org/10.14324/111.9781911576938, 2018.

BouDagher-Fadel, M. K. and Banner, F. T.: Revision of the stratigraphic significance of the Oligocene-Miocene "Letter-Stages", Rev. Micropaléontol., 42, 93–97, https://doi.org/10.1016/S0035-1598(99)90095-8, 1999.

BouDagher-Fadel, M. K. and Price, G. D.: Evolution and paleogeographic distribution of the Lepidocyclinids, J. Foramin. Res., 40, 79–108, https://doi.org/10.2113/gsjfr.40.1.79, 2010.

BouDagher-Fadel, M. K. and Price, G. D.: The phylogenetic and palaeogeographic evolution of the miogypsinid larger benthic foraminifera, J. Geol. Soc., 170, 185–208, https://doi.org/10.1144/jgs2011-149, 2013.

BouDagher-Fadel, M. K. and Price, G. D.: The phylogenetic and palaeogeographic evolution of the nummulitoid larger benthic foraminifera, Micropaleontology, 60, 483–508, 2014.

BouDagher-Fadel, M. K. and Price, G. D.: The geographic, environmental and phylogenetic evolution of the Alveolinoidea from the Cretaceous to the present day, UCL Open Environment, 2, 1–34, https://doi.org/10.14324/111.444/ucloe.000015, 2021.

Boukhary, M., Kuss, J., and Abdelraouf, M.: Chattian larger foraminifera from Risan Aneiza, northern Sinai, Egypt, and implications for Tethyan paleogeography, Stratigraphy, 5, 179–192, 2008.

Bover-Arnal, T., Ferràndez-Cañadell, C., Aguirre, J., Esteban, M., Ferràndez-Carmona, J., Albert-Villanueva, E., and Salas, R.: Late Chattian platform carbonates with benthic foraminifera and coralline algae from the SE Iberian Plate, Palaios, 32, 61–82, https://doi.org/10.2110/palo.2016.007, 2017.

Brunn, J. H., Chevalier, J.-P., and Marie, P.: Quelques formes nouvelles de Polypiers et de Foraminifères de l'Oligocene et du Miocene du NW de la Grèce. II. Foraminifères, Bull. Soc. géol. Fr., 5, 193–205, https://doi.org/10.2113/gssgfbull.S6-V.1-3.193, 1955.

Buxton, M. W. N. and Pedley, H. M.: A standardized model for Tethyan Tertiary carbonate ramps, J. Geol. Soc. London, 146, 746–748, https://doi.org/10.1144/gsjgs.146.5.0746, 1989.

Cahuzac, B. and Poignant, A.: Essai de biozonation de l'Oligo–Miocène dans les bassins européens à l'aide des grands foraminifères néritiques, Bull. Soc. géol. Fr., 168, 155–169, 1997.

Cahuzac, B. and Poignant, A.: Larger benthic foraminifera (Neogene), in: Mesozoic and Cenozoic sequence chronostratigraphic framework of European basins, edited by: Hardenbol, J., Thierry, J., Farley, M. B., Jacquin, T., de Graciansky, P. C., and Vail, P., S.E.P.M., spec. publ. 60, Appendix, 766, https://doi.org/10.2110/pec.98.02.0003, 1998.

Cahuzac, B. and Poignant, A.: Les foraminifères du Burdigalienne moyen à supérieur de la région sud-aquitaine (Golfe de Saubrigues, SW France), Rev. Micropaléontol., 47, 153–192, https://doi.org/10.1016/j.revmic.2004.10.003, 2004.

Carozzi, A. V., Reyes, M. V., and Ocampo, V. P.: Microfacies and microfossils of the Miocene reef carbonates of the Philippines, Philippine Oil Development Comp., spec. publ. 1, 1–79, 1976.

Cohen, K. M., Harper, D., Gibbard, P., and Car, N.: The ICS international chronostratigraphic chart this decade, Episodes, 48, 105–115, https://doi.org/10.18814/epiiugs/2025/025001, 2025.

Defrance, J. L. M.: Lenticulite (Foss.), in: Dictionnaire des Sciences Naturelles, volume 25, edited by: Cuvier, F., Levrault, Strasbourg & Le Normant, Paris, 452–453, 1822.

de Mulder, E. F. J.: Microfauna and sedimentary-tectonic history of the Oligo–Miocene of the Ionian Islands and western Epirus (Greece), Utrecht Micropal. Bull., 13, 1–139, 1975.

Douvillé, H.: Revision des Lépidocyclines. Deuxieme partie, Soc. géol. Fr., mém. n. ser. 2, 51–115, 1925.

Douvillé, R.: Observations sur les faunes à Foraminifères du sommet du Nummulitique italien, Bull. Soc. Géol. Fr., 8, 88–95, 1908.

Drooger, C. W.: Transatlantic correlation of the Oligo–Miocene by means of foraminifera, Micropaleontology, 2, 183–192, https://doi.org/10.2307/1484102, 1956.

Drooger, C. W.: Radial Foraminifera; morphometrics and evolution, Verh. Koninkl. Nederl. Akad. Wetensch. Afd. Natuurk., 41, 1–242, https://doi.org/10.2113/gsjfr.24.4.312, 1993.

Drooger, C. W. and Laagland, H.: Larger foraminiferal zonation of the European Mediterranean Oligocene, Proc. Kon. Ned. Ak. Wet., ser. B, 89, 135–148, 1986.

Drooger, C. W. and Socin, C.: Miocene foraminifera from Rosignano, Northern Italy, Micropaleont., 5, 415–426, https://doi.org/10.2307/1484126, 1959.

Drooger, C. W., Marks, P., and Papp, A.: Smaller radiate *Nummulites* of northwestern Europe, Utrecht Micropal. Bull., 5, 1–137, 1971.

Fallot, P.: Estudios geológicos en la Zona Subbética entre Alicante y el Río Guadiana Menor, Cons. Sup. Inv. Cient. Inst. "Lucas Mallada", Madrid, 719 pp., 1945.

Ferràndez-Cañadell, C. and Bover-Arnal, T.: Late Chattian larger foraminifera from the Prebetic domain (SE Spain): new data on Shallow Benthic Zone 23, Palaios, 32, 83–109, https://doi.org/10.2110/palo.2016.010, 2017.

Foucault, A.: Sur la tectonique de la zone subbetique de la region de Huescar (prov. de Grenade, Espagne) et sur son Nummulitique, Bull. Soc. géol. Fr., S7-II, 318–321, https://doi.org/10.2113/gssgfbull.S7-II.3.318, 1960.

Foucault, A.: Étude géologique des environs des sources du Guadalquivir, provinces de Jaén et de Grenade, Espagne méridionale. Sciences de la Terre, Université Pierre et Marie Curie, Paris VI, 1971.

Foucault, A.: Travaux et titres scientifiques et universitaires, Paris, 36 pp., 1974.

Galindo-Zaldívar, J., Braga, J. C., Marín-Lechado, C., Ercilla, G., Martín, J. M., Pedrera, A., Casas, D., Aguirre, J., Ruiz-Constán, A., Estrada F., Puga-Bernadéu, Á., Sanz de Galdeano, C., Juan, C., García-Alix, A., Vázquez, J. T., and Alonso, B.: Extension in the Western Mediterranean, in: The Geology of Iberia: a geodynamic approach. Regional Geology Reviews, 4, Ceno-

zoic Basins, edited by: Quesada, C. and Oliveira, J. T., Springer Nature, Switzerland, 61–103, https://doi.org/10.1007/978-3-030-11190-8_3, 2019.

García-Hernández, M., López-Garrido, A. C., Rivas, P, Sanz de Galdeano, C., and Vera, J. A.: Mesozoic palaeogeographic evolution of the external zones of the Betic Cordillera, Geol. Mijnbouw., 59, 155–168, 1980.

Geel, T.: Recognition of stratigraphic sequences in carbonate platform and slope deposits: empirical models based on microfacies analysis of Palaeogene deposits in southeastern Spain, Palaeogeogr. Palaeoclimatol. Palaeoecol., 155, 211–238, https://doi.org/10.1016/S0031-0182(99)00117-0, 2000.

Ghafor, I. M.: Evolutionary aspects of *Lepidocyclina* (*Nephrolepidina*) from Baba Formation (late Oligocene) in Bai-Hassan well-25, Kirkuk area, Northeast Iraq, Arab. J. Geosci., 8, 9423–9431, https://doi.org/10.1007/s12517-015-1865-9, 2015.

Greig, D. A.: *Rotalia viennoti*, an important foraminiferal species from Asia Minor and Western Asia, J. Paleontol., 9, 523–526, https://www.jstor.org/stable/1298200 (last access: 20 November 2025), 1935.

Harzhauser, M., Landau, B., Mandic, O., and Neubauer, T.: The Central Paratethys Sea – rise and demise of a Miocene European marine biodiversity hotspot, Sci. Rep., 14, 6288, https://doi.org/10.1038/s41598-024-67370-6, 2025.

Henson, F. R. S.: Larger Foraminifera from Aintab, Turkish Syria, Eclogae geol. Helv., 30, 45–57, https://doi.org/10.5169/seals-159717, 1937.

Hohenegger, J.: Coenoclines of larger foraminifera, Micropaleontology, 46, 127–151, https://doi.org/10.2113/0340009, 2000.

Hohenegger, J. and Yordanova, E.: Depth–transport functions and erosion–deposition diagrams as indicators of slope inclination and time-averaged traction forces: applications in tropical reef environments, Sedimentology, 48, 1025–1046, https://doi.org/10.1046/j.1365-3091.2001.00407.x, 2001.

Hottinger, L.: Recherches sur les Alvéolines du Paléocène et de l'Éocène, Mém. Suisses Paléont., 75–76, 1–243, 1960.

Hottinger, L.: Foraminifères Operculiniformes, Mém. Mus. Nati. Hist. Nat., 57, 1–159, ISBN 2-85653-028-1, 1977.

Hottinger, L.: Shallow benthic foraminiferal assemblages as signals for depth of their deposition and their limitations, Bull. Soc. géol. Fr., 168, 491–505, 1997.

Hottinger, L.: The depth-depending ornamentation of some lamellar-perforate foraminifera, Symbiosis, 42, 141–151, 2006.

Hottinger, L.: *Neorotalia* Bermúdez, 1952, in: Paleogene larger Rotaliid Foraminifera from the Western and Central Neotethys, edited by: Bassi, D., Berlin, Springer International Publishing Switzerland, 153–157, https://doi.org/10.1007/978-3-319-02853-8, 2014.

Hottinger, L., Lehman, R., and Schaub, H.: Données actuelles sur la biostratigraphie du Nummulitique Méditerranéen, Colloque sur le Paléogène, Bordeaux 1962, Mém. B.R.G.M., 28, 611–652, 1964.

Hottinger, L., Halics, E., and Reiss, Z.: The foraminiferal genera *Pararotalia*, *Neorotalia*, and *Calcarina*: taxonomic revision, J. Paleontol., 65, 18–33, https://doi.org/10.1017/S0022336000020151, 1991.

Iaccarino, S.: Mediterranean Miocene and Pliocene planktic foraminifera, in: Plankton Stratigraphy 1, edited by: Bolli, H. M., Saunders, J. B., and Perch-Nielsen, K., Cambridge University Press, 283–314, 1985.

Jabaloy, A., Padrón-Navarta, J. A., Gómez-Pugnaire, M. T., López Sánchez-Vizcaíno, V., and Garrido, C. J.: Alpine orogeny: deformation and structure in the Southern Iberian Margin (Betics sl), in: The Geology of Iberia: a geodynamic approach. Volume 3: The Alpine Cycle, edited by: Quesada, C. and Oliveira, J. T., Springer International Publishing Nature, 453–486, https://doi.org/10.1007/978-3-030-11295-0_10, 2019.

Jeong, S. Y., Nelson, W. A., Sutherland, J. E., Peña, V., Le Gall, L., Diaz-Pulido, G., Won, B. Y., and Cho, T. O.: Corallinapetrales and corallinapetraceae: a new order and new family of coralline red algae including *Corallinapetra gabriellii* comb. nov., J. Phycol., 57, 849–862, https://doi.org/10.1111/jpy.13115, 2021.

Joly, N. and Leymerie, A.: Mémoire sur les Nummulites, considérées zoologiquement et géologiquement, Mém. Acad. Sci. Toulouse, 4, 149–218, 1848.

Kennett, J. P. and Srinivasan, M. S.: Neogene planktonic foraminifera. A phylogenetic atlas, Hutchinson Ross Publishers, Stroudsburg, Pa., 265 pp., 1983.

Langer, M. R. and Hottinger, L.: Biogeography of selected larger Foraminifera, Micropaleontology, 46, 105–126, 2000.

Lemoine, P. and Douvillé, R.: Sur le genre *Lepidocyclina* Gümbel, Mém. Soc. géol. Fr., sér. 12, 32, 1–41, 1904.

Less, G.: Paleontology and stratigraphy of the European Orthophragminae, Geol. Hung., ser. Palaeontol., 51, 1–373, 1987.

Less, G.: Upper Oligocene larger foraminifers of the Bükk Mountains (NE Hungary), Magyar Állami Földtani Intézet Évi Jel., 1989, 411–465, 1991.

Less, G.: The late Paleogene larger foraminiferal assemblages of the Bükk Mountains (NE Hungary), Rev. Españ. Micropaleontol., 31, 347–356, 1999.

Less, G. and Özcan, E.: The late Eocene evolution of nummulitid foraminifer *Spiroclypeus* in the Western Tethys, Acta Palaeont. Pol., 53, 303–316, https://doi.org/10.4202/app.2008.0211, 2008.

Less, G., Kertész, B., and Özcan, E.: Bartonian to end-Rupelian reticulate *Nummulites* of the Western Tethys, Ann. Inst. Geosci., 29, 344–345, 2006.

Less, G., Báldi-Beke, M., Pálfalvi, S., Földessy, J., and Kertész, B.: New data on the age of the Recsk volcanics and of the adjacent sedimentary rocks, Proc. Univ. Miskolc, Series A, Mining, 73, 57–84, 2008.

Less, G., Özcan, E., and Okay, A. I.: Stratigraphy and larger foraminifera of the Middle Eocene to Lower Oligocene shallow-water marine units in the northern and eastern parts of the Thrace Basin, NW Turkey, Turk. J. Earth Sci., 20, 793–845, https://doi.org/10.3906/yer-1010-53, 2011.

Less, G., Frijia, G., Özcan, E., Saraswati, P. K., Parente, M., and Kumar, P.: Nummulitids, lepidocyclinids and Sr-isotope data from the Oligocene of Kutch (western India) with chronostratigraphic and paleobiogeographic evaluations, Geodin. Acta, 30, 183–211, https://doi.org/10.1080/09853111.2018.1465214, 2018.

Lirer, F., Foresi, L. M., Iaccarino, S. M., Salvatorini, G., Turco, E., Cosentino, C., Sierro, F. J., and Caruso, A.: Mediterranean Neogene planktonic foraminifer biozonation and biochronology, Earth-Sci. Rev., 196, 102869, https://doi.org/10.1016/j.earscirev.2019.05.013, 2019.

Lupiani-Moreno, E., Roldán-García, F. J., and Villalobos-Megía, M.: Mapa geológico de España a escala 1:50.000 y memo-

ria, Plan MAGNA, Hoja 929 (Canal de San Clemente), IGME, 1994a.

Lupiani-Moreno, E., Roldán-García, F. J., and Villalobos-Megía, M.: Mapa geológico de España a escala 1:50.000 y memoria, Plan MAGNA, Hoja 950 (Huéscar), IGME, 1994b.

Lunt, P. and Allan, T.: Larger foraminifera in Indonesian biostratigraphy, calibrated to isotopic dating, Geol. Res. Dev. Cent. Mus., Workshop on Micropalaeontology, Bandung, 1–109, 2004.

Lunt, P. and Renema, W.: On the *Heterostegina–Tansinhokella–Spiroclypeus* lineage(s) in SE Asia, Berita Sedimentol., 30, 6–31, https://journal.iagi.or.id/index.php/FOSI/article/view/132 (last access: 20 November 2025), 2014.

Martini, E.: Standard Tertiary and Quaternary calcareous nannoplankton zonation, Proc. 2nd. Plankt. Conf., Rome 1970, 2, Tecnoscienza, Roma, 739–786, 1971.

Michelotti, G.: Saggio storico dei Rizopodi caratteristici dei terreni sopracretacei, Mem. Mat. Fis. Soc. It. Sci. Modena, 22 (Fisica), 253–302, 1841.

Michelotti, G.: Études sur le Miocène inférieur de l'Italie septentrionale, Natuurk. Verh. Holl. Maatsch. Wetensch. Haarlem., ser. 2, 14, 1–183, 1861.

Özcan, E. and Less, G.: First record of the co-occurrence of western Tethyan and Indo-Pacific larger foraminifera in the Burdigalian of the Mediterranean province, J. Foramin. Res., 39, 23–39, https://doi.org/10.2113/gsjfr.39.1.23, 2009.

Özcan, E., Less, G., Báldi-Beke, M., Kollányi, K., and Acar, F.: Oligo–Miocene foraminiferal record (Miogypsinidae, Lepidocyclinidae and Nummulitidae) from the Western Taurides (SW Turkey): biometry and implications for the regional geology, J. Asian Earth Sci., 34, 740–760, https://doi.org/10.1016/j.jseaes.2008.11.002, 2009a.

Özcan, E., Less, G., and Baydogan, E.: Regional implications of biometric analysis of lower Miocene larger foraminifera from central Turkey, Micropaleontology, 55, 559–588, 2009b.

Özcan, E., Less, G., Báldi-Beke, M., and Kollányi, K.: Oligocene hyaline larger foraminifera from Keleresdere section (Mus, Eastern Turkey), Micropaleontology, 56, 465–493, 2010.

Parente, M. and Less, G.: Nummulitids, lepidocyclinids and strontium isotope stratigraphy of the Porto Badisco Calcarenite (Salento Peninsula, southern Italy). Implications for the biostratigraphy and paleobiogeography of Oligocene larger benthic foraminifera, It. J. Geosci., 138, 2391–261, https://doi.org/10.3301/IJG.2019.04, 2019.

Peña, V., Vieira, C., Braga, J. C., Aguirre, J., Rösler, A., Baele, G., De Clerck, O., and Le Gall, L.: Radiation of the coralline red algae (Corallinophycidae, Rhodophyta) crown group as inferred from a multilocus time-calibrated phylogeny, Mol. Phylogenetics Evol., 150, 106845, https://doi.org/10.1016/j.ympev.2020.106845, 2020.

Perrin, C. and Bosellini, F. R.: Paleobiogeography of scleractinian reef corals: changing patterns during the Oligocene–Miocene climatic transition in the Mediterranean, Earth-Sci. Rev., 111, 1–24, https://doi.org/10.1016/j.earscirev.2011.12.007, 2012.

Piller, W. E., Harzhauser, M., Kranner, M., Mandic, O., Mohtat, T., and Daneshian, J.: The Tethyan Seaway during the early to middle Miocene – New data and a review, Gondwana Res., 135, 57–74, https://doi.org/10.1016/j.gr.2024.08.004, 2024.

Reiss, Z. and Hottinger, L.: The Gulf of Aqaba: ecological micropaleontology, Ecological Studies, 50, Springer-Verlag, Berlin, 1–354, https://doi.org/10.1007/978-3-642-69787-6, 1984.

Renema, W.: Fauna development of larger benthic foraminifera in the Cenozoic of Southeast Asia, in: Biogeography, time and place: distributions, barriers and islands, edited by: Renema, W., Springer-Verlag, Berlin, 179–215, https://doi.org/10.1007/978-1-4020-6374-9_6, 2007.

Reuter, M., D'Olivo, J. P., Brachert, T. C., Spreter, P. M., Mertz-Kraus, R., and Wrozyna, C., Mid-Miocene warmth pushed fossil coral calcification to physiological limits in high-latitude reefs, Commun. Earth Environ., 6, 569, https://doi.org/10.1038/s43247-025-02559-9, 2025.

Sanz de Galdeano, C. and Vera, J. A.: Stratigraphic record and palaeogeographical context of the Neogene basins in the Betic Cordillera, Spain, Basin Res., 4, 21–36, https://doi.org/10.1111/j.1365-2117.1992.tb00040.x, 1992.

Sanz de Galdeano, C. and Alfaro, P.: Tectonic significance of the present relief of the Betic Cordillera, Geomorphology, 63, 178–190, https://doi.org/10.1016/j.geomorph.2004.04.002, 2004.

Schaub, H.: *Nummulites* et *Assilina* de la Téthys palèogène. Taxinomie, phylogenèse et biostratigraphie, Mem. Suisses Paléontol., 104–106, 1–23, 1981.

Serra-Kiel, J., Hottinger, L., Caus, E., Drobne, K., Ferrández, C., Jauhri, A. K., Less, G., Pavlovec, R., Pignatti, J., Samsó, J. M., Schaub, H., Sirel, E., Strougo, A., Tambareau, Y., Tosquella, J., and Zakrevskaya, E.: Larger foraminiferal biostratigraphy of the Tethyan Paleocene and Eocene, Bull. Soc. géol. Fr., 169, 281–299, 1998.

Serra-Kiel, J., Gallardo-Garcia, A., Razin, P. H., Robinet, J., Roger, J., Grelaud, C., Leroy, S., and Robin, C.: Middle Eocene–Early Miocene larger foraminifera from Dhofar (Oman) and Socotra Island (Yemen), Arab. J. Geosci., 9, 344, https://doi.org/10.1007/s12517-015-2243-3, 2016.

Serra-Kiel, J., Vicedo, V., Baceta, J. I., Bernaola, G., and Robador, A.: Paleocene larger foraminifera from Pyrenean basin with a recalibration of the Paleocene Shallow Water Zones, Geol. Acta, 18.8, 1–69, https://doi.org/10.1344/GeologicaActa2020.18.8, 2020.

Silvestri, A.: Review of: Douvillé, H., Les foraminifères dans le Tertiaire des Philippines, Riv. Ital. Pal., 18, 55–59, 1912.

Simmons, M. D.: Larger benthic foraminifera. Subchapter 3H, in: Geologic Time Scale 2020, edited by: Gradstein, F. M., Ogg, J. G. Schmitz, M. D., and Ogg, G. M., Elsevier, Amsterdam, 88–98, ISBN 10.0128243600,2020.

Sirotti, A.: Phylogenetic classification of Lepidocyclinidae: a proposal, Boll. Soc. Paleontol. It., 21, 99–112, 1982.

Todd, R. and Post, R.: Smaller foraminifera from Bikini drill holes, U.S. Geol. Surv. Prof. Pap., 260-n, 547–568, 1954.

Tomassetti, L., Petracchini, L., Brandano, M., Trippetta, F., and Tomassi, A.: Modelling lateral facies heterogeneity of an upper Oligocene carbonate ramp (Salento, southern Italy), Mar. Petrol. Geol., 96, 254–270, https://doi.org/10.1016/j.marpetgeo.2018.06.004, 2018.

van der Vlerk, I. M.: Modification de l'ontogénèse pendant l'évolution des lépidocyclines, Bull. Soc. géol. Fr., 7, 669–673, 1959.

van Heck, S. E. and Drooger, C. W.: Primitive *Lepidocyclina* from San Vicente de la Barquera (N. Spain), Proc. Kon. Ned. Ak. Wet., ser. B, 87, 301–318, 1984.

Vannucci, G., Basso, D., and Fravega, P.: New observations on the anatomy of the fossil calcareous alga *Subterraniphyllum* Elliott, Riv. It. Paleont., 106, 237–246, https://doi.org/10.13130/2039-4942/5400, 2000.

Wade, B. S., Pearson, P. N., Berggren, W. A., and Pälike, H.: Review and revision of Cenozoic tropical planktonic foraminiferal biostratigraphy and calibration to the geomagnetic polarity and astronomical time scale, Earth-Sci. Rev., 104, 111–142, https://doi.org/10.1016/j.earscirev.2010.09.003, 2011.

Wade, B. S., Olsson, R. K., Pearson, P. N., Huber, B. T., and Berggren, W. A. (Eds.): Atlas of Oligocene planktonic foraminifera, Cushman Foundation for Foraminiferal Research, Cushman Spec. Publ. 46, ISBN (electronic) 9781970168419, 2018.

Wielandt-Schuster, U.: Neogene larger foraminifera of the Mesohellenic Basin, Greece, Cour. Forsch.-Inst. Senckenb., 248, 183–225, 2004.

Yordanova, E. K. and Hohenegger, J.: Taphonomy of larger foraminifera; relationships between living individuals and empty tests on flat reef slopes (Sesoko Island, Japan), Facies, 46, 29–34, https://doi.org/10.1007/BF02668080, 2002.

Young, J. R., Wade, B. S., and Huber B. T.: pforams@mikrotax website, 21 Apr. 2017, https://www.mikrotax.org/pforams (last access: 20 November 2025), 2017.